Pittsburg State University

Pittsburg State University Digital Commons

Electronic Thesis Collection

Summer 7-10-2019

SYNTHESIS OF NEW ALIPHATIC PSEUDO-BRANCHED POLYESTER CO-POLYMERS FOR BIOMEDICAL APPLICATIONS

Zachary Shaw
Pittsburg State University, zachary.shaw@gus.pittstate.edu

Follow this and additional works at: https://digitalcommons.pittstate.edu/etd

Part of the Biotechnology Commons, Nanomedicine Commons, and the Polymer Chemistry Commons

SYNTHESIS OF NEW ALIPHATIC PSEUDO-BRANCHED POLYESTER CO-POLYMERS
FOR BIOMEDICAL APPLICATIONS

A Thesis Submitted to the Graduate School
in Partial Fulfillment of the Requirements
For the Degree of
Master of Science in Polymer Chemistry

Zachary Shaw

Pittsburg State University

Pittsburg, Kansas

May, 2019

SYNTHESIS OF NEW ALIPHATIC PSEUDO-BRANCHED POLYESTER CO-POLYMERS
FOR BIOMEDICAL APPLICATIONS

Zachary Shaw

APPROVED:

Thesis Advisor

Dr. Santimukul Santra, Department of Chemistry

Committee Member

Dr. Tuhina Banerjee, Department of Chemistry

Committee Member

Dr. Irene Zegar, Department of Chemistry

Committee Member

Dr. Jian Hong, Kansas Polymer Research Center

ACKNOWLEDGEMENTS

First, I would like to say thank you to Dr. Santimukul Santra and Dr. Tuhina Banerjee for accepting me as a member and graduate researcher of their lab, for the opportunity to do exciting and forefront research in nanotherenostics and polymer chemistry, and for their financial assistance in the pursuit of my master's degree. I would also like to thank PSU's Polymer Chemistry Initiative for its financial aid, and for the job as a graduate teaching assistant. Both positions gave me valuable experiences that I will benefit from in pursuit of my Ph.D.

I would like to thank all those at the Kansas Polymer Research Center for their aid in learning to use characterization equipment including but not limited to GPC, DSC, and TGA located there, and the chemistry department faculty for their assistance. Thank you Dr. Petar Dvornic, Alisa Zlatanic, Dr. James McAfee, Dr. Jody Neef, and Mei, for your continued support, encouragement, and assistance during my project.

I would also like to thank my committee members Dr. Santra, Dr. Banerjee, Dr. Irene Zegar, and Dr. Jian Hong for their time and the work they did going over and revising my thesis. Without their assistance and support, I would not have gotten thus far.

Last and most important, I would like to thank my core support Jessica (my better half), my family, friends, lab-mates, and one of my best friends, my colleague and roommate Ren for their unwavering emotional support and encouragement in the completion of my degree. Without their help, I would not have been able to attain this achievement.

SYNTHESIS OF NEW ALIPHATIC PSEUDO-BRANCHED POLYESTER CO-POLYMERS
FOR BIOMEDICAL APPLICATIONS

An Abstract of the Thesis by
Zachary Shaw

In this study, a hyperbranched polyester co-polymer was designed using a proprietary monomer and diethylene glycol or triethylene glycol as monomers. The synthesis was carried out using standard melt polymerization technique and catalyzed by ρ-Tolulenesulfonic acid. The resulting polymers were purified using the solvent precipitation method and characterized using various chromatographic and spectroscopic methods including GPC, MALDI-TOF, and NMR. We have observed polymers with a molecular weight of 29,643 kDa and 33,996 kDa, a molecular weight ideal for drug delivery systems. Thus, these polymers were chosen for further modification into folate-functionalized polymeric nanoparticles for targeted drug delivery to LNCaP prostate cancer cells. We hypothesized that due to the 3D structure of the diacid A_2B monomer, we expect a pseudo-branched polymer that is globular in shape which will be ideal for drug carrying and delivery. We used a solvent diffusion method, wherein the polymer can be simultaneously converted into water-dispersible nanoparticles and therapeutic agents (doxorubicin) can be encapsulated into the polymeric nanocavities. The efficacy of this delivery system was gauged by treating LNCaP prostate cancer cells with the drug-loaded nanoparticles and assessing the results of the treatment. The results were analyzed by cytotoxicity (MTT) assays, drug release studies, and confocal and fluorescence microscopy. The experimental results collectively show a nanoparticle that was biocompatible, target-specific, and successfully initiated apoptosis in an *in vitro* prostate cancer cell model.

Keywords: Nanoparticle · Cancer · Polyester · Biocompatible · Nanomedicine · Targeted Delivery

TABLE OF CONTENTS

LIST OF SCHEMES

LIST OF FIGURES

Chapter I

Introduction

Most individuals' understanding of polymers is nothing more than the "plastic" items they use throughout their day to day lives. This day and age, these "plastics" are ever evolving on a daily basis to materials that go beyond the narrowly descriptive term "plastic" thanks to the talented chemists around the world, as the demand for new materials is ever increasing. Because of this, the field of polymer science is developing into a multi-faceted discipline with many overlapping fields. One such discipline is bio-nanotechnology in the field of medicine.

The development of nanotechnology has sparked an evolution within the field of medicine from traditional systemic administration to targeted, micro-precise dosing of therapeutic compounds. This new technology is known as nanomedicine and has the potential to completely change how we diagnose, treat, and prevent disease or illness. Nanomedicine is made from a tunable, bio-degradable/compatible polymer which can encapsulate a variety of drugs, dyes, and other therapeutic molecules, along with a surface modification to attach ligands for targeted delivery. In the interest of their patients, doctors using a lower dose would be able to achieve the same IC_{50} values as they would using systemic dosages of highly toxic chemotherapy drugs that generally lower a person's quality of life due to side effects like nausea, pain, and hair loss. Using targeted delivery, patients could experience less of these side effects, which is especially vital in end-stage cancer where a patient is weighing the cost of the side effects of the

drugs vs. how much longer it will prolong their life. Knowing the side effects will be significantly reduced, patients can make that decision a little easier using nanomedicine as targeted delivery.

Nanomedicine is a new and promising innovation of chemistry in the field of medicine. New compounds can be synthesized using commercially available chemicals to make bio-compatible polymers for use in nanomedicine. For compounds to be biocompatible, they must be non-toxic to the patient and must perform their function and be eliminated by the body without issue. The resulting bio-compatible polymer must be able to be further functionalized with targeting ligands, converted to a stable nanoparticle solution, successfully encapsulate its payload, and it must also be stable in storage until after administration when it is taken in through endocytosis by the target cell.

Previously researchers have shown where hyperbranched polyester (HBPE) polymers were successfully used as therapeutic payload delivery systems for the treatment of cancer cells utilizing a proprietary A_2B monomer structure, for the first time. This first generation HBPE polymer was advantageous in that it was tunable, multi-functional, biodegradable, and encapsulated various hydrophobic payloads.[1] In the interest of further developing this type of HBPE polymer, the introduction of hydrophilic moieties into the polymer network will make the polymer nanocavities more amphiphilic, which can allow for the encapsulation of both hydrophobic and hydrophilic drugs. These hydrophilic moieties would also increase the internal nanocavity volume, allowing for the encapsulation of a larger payload.

The focus of this thesis is the synthesis of the said polymer, where hydrophilicity was incorporated into the polymer network by the co-condensation of triethylene glycol or diethylene glycol with a proprietary A_2B monomer. Diethylene glycol and triethylene glycol were chosen due to their high solubility in water, and the presence of polar groups in the backbone will allow for

the encapsulation of more polar molecules. They also act as a "chain extender" to the proprietary A$_2$B monomer which will increase the size of the nanocavities within the polymer. Due to the carboxylic acid groups in the proprietary monomer, the polymer surface will allow for easy functionalization of the targeting ligand and its ultimate stability in water as a nanoparticle solution.

Once the HBPE was synthesized and further modified to a nanoparticle solution, the payload consisting of chemotherapeutic drug doxorubicin and DiI optical dye were encapsulated by the polymer within the nanocavities present in the polymer network. The nanoparticles were studied for their encapsulation efficiency and were incubated with the LNCaP prostate cancer cell line to determine the effectiveness of this targeted delivery system. Results will determine if the proposed delivery system can effectively encapsulate a therapeutic payload and can selectively deliver that payload to treat cancer, or if this system needs to be modified or improved for further in-vivo studies.

Chapter II

Literature Review

The Foundation of Polymers

Polymers are described as compounds made up of polymerized, repeating structural units called monomers.[2,3] Polymers are found everywhere, occurring both naturally and synthetically. The inception of the field of polymer science began with a German chemist named Hermann Staudinger, who published the existence of polymers in 1920 with an idea to link numerous monomers together by covalent bonds to design high molecular weight structural and functional polymers.[4,5]

Staudinger's idea was met with skepticism from his colleagues. Then, it was thought that polymers above 5,000 g/mol were not due to covalent linking of monomers, but due to molecules aggregating as a colloid.[6] Almost twenty years later, two other chemists, Wallace Carothers, and Herman Mark made discoveries that supported Staudinger's claim. In 1953 Staudinger was awarded the Nobel Prize (more than 30 years after the fact), for his famous macromolecular theory of polymers. These three scientists elucidated the field of polymer science and from which was built. Polymer science is now a broad discipline, with many technologically essential innovations in materials. Due to their breadth, polymers can be classified based on a number of their features including origin, monomer species, and skeletal structure.[7]

<u>Polymer Classification</u>

One way polymers can be classified according to their origin is as a natural polymer, meaning the polymer is made by nature. There are several different natural polymers found in nature such as cellulose from plants, natural rubber from the latex of the rubber tree, silk from a silkworm, and DNA and proteins from living organisms.[8] Not every natural polymer is easily degradable, and for this reason their use in biological systems is limited. Scientists wanted to find ways to use natural polymers in biological systems. Natural polymers can be synthetically modified to give them new or more enhanced properties. These new polymers can be categorized as semi-synthetic polymers. Compounds like natural proteins and polysaccharides have been used as hydrogels and scaffolds for tissue engineering and gene delivery.[9,10] The natural compounds collagen and hyaluronic acid were blended with poly(vinyl alcohol) (PVA) and poly(acrylic acid) (PAA) in different ratios to develop a delivery system for growth hormone using a combination of natural and synthetic polymers.[11] The final polymer origin classification is fully synthetic polymers. Synthetic polymers are merely macromolecules designed to have properties for particular uses. Due to the large interest in synthetic polymers, there is a vast collection of new polymers with fascinating properties. For example, due to its good degradability and biocompatibility, synthetic poly(lactic-co-glycolic acid) (PLGA) has been used to make 3D scaffolds for growing breast cancer.[12] The synthetic polymer polyethylene glycol (PEG) is also used in the synthesis of synthetic biomaterials. A monomethoxyl poly(ethylene glycol)-block-poly(N,N′-diethylaminoethyl methacrylate) (mPEG-b-PDEA) polymer was designed as a drug delivery system sensitive to redox chemistry.[13]

Polymers can also be classified according the makeup of their monomer species. A polymer can be a homopolymer, a copolymer, or a graft polymer. Additionally, a polymer can be

aliphatic or aromatic within its backbone and or its substituents. Homopolymers can be broadly used to classify polymers whose makeup is a single type of structural unit.[7] The following classification is co-polymers, defined as polymers that contain more than one type of repeat unit. Co-polymers can be further described as being a statistical or a random copolymer. For example, a copolymer with substituents A and B can arrange themselves in an alternating -A-B- pattern, or they can be in the form of a block copolymer where a polymer block of substituent A (-A-A-A-) reacts with a polymer block of substituent B (-B-B-B-) in a repeating pattern. In a random polymer, the substituents are arranged in no particular order. Graft polymers are associated with polymers that have a homopolymer backbone with pendant branches of another homopolymer.[8]

Polymers are also grouped by the type of primary structure the polymer backbone forms. They can be considered either a linear polymer or a dendritic polymer. A linear polymer indicates the backbone is made up of a chain of monomeric units with two terminal groups. Dendritic polymers can be further classified as a true dendrimer or a hyperbranched polymer. Monomers that make these polymers have multifunctional moieties, such as an A_2B or an AB_2 system, which allows for branching. With true dendrimers, the degree of branching is a strictly controlled, multi-step method where a monodisperse polymer is made.[14] Hyperbranched polymers are often made in a single-step method are polydisperse, and the degree of branching has some control.[15] Due to these advantages, dendritic polymers have stronger theranostic applications over linear polymers, which have limited surface functionality, lower encapsulation efficiency, and uncontrolled drug release.[16]

The Significance of Dendritic Polymers in Drug Delivery

There are very few natural macromolecular structures that are dendritic, and those that are natural are generally biological compounds like glycans and pectins are hyperbranched structures. True dendrimers are made synthetically and are a major class of macromolecular structure characterization.[17] They are very symmetrical, perfectly branched, three dimensional, globular structures and are made up of three components: the interior dendrimer (which houses the core molecule), and the outer shell surrounding it. The core molecule controls the interior dendrimer pore size which controls the type and size of cargo molecules. The interior dendrimer contains the pores where the therapeutic cargo is held. The outer core is functional/can be functionalized with various chemistries for targeting ligands and or solubility.[18]

Due to the very costly and lengthy synthesis of true dendrimers, similar globular like three-dimensional polymers termed hyperbranched polymers were considered. These polymers were advantageous in that they were a one-pot synthesis, cost-effective, and synthesis time was not excessive. Also, these polymers have multifunctional surfaces to allow for easy surface modification and high drug loading efficiencies.[15] These attributes, in addition to several other properties make hyperbranched polymers a viable substitute to true dendrimers for use as a drug delivery system.

When developing a polymer for use as a drug delivery vehicle, care must be taken in its design so that no toxic byproducts are produced by its degradation to ensure maximum
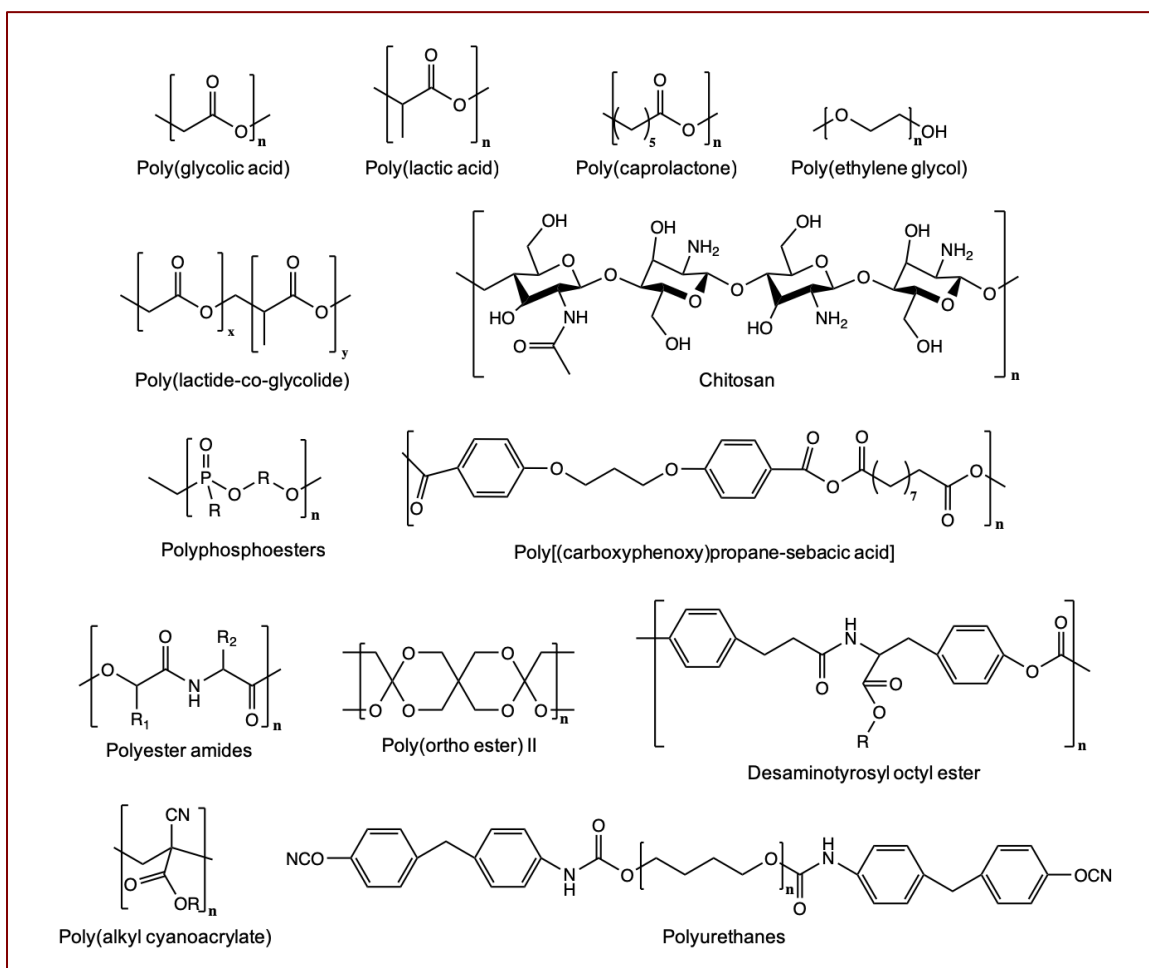
Figure 1:Polymers used in drug delivery that are known to be hydrolysable and further biodegradable.[19]

biocompatibility. For a compound to be biodegradable, it must have bonds that can be

hydrolyzed and must degrade under redox or low pH conditions while producing no cytotoxic

byproducts. There are several varieties of polymers with this type of chemistry and are listed in

Figure 1. One such example is an ester group. The ester bond can be easily hydrolyzed by natural

enzymes called esterases naturally present in human tissue.[20]

Due to their known biodegradability, synthetic adaptability, and high molecular weight,

aliphatic polyesters are of great use as drug delivery systems.[21] Dr. Santra designed and

synthesized a novel, custom aliphatic diacid monomer to be polymerized to an aliphatic

hyperbranched polyester for use in the formulation of nanoparticles for drug delivery. This

monomer was novel in that it was the first of its kind to utilize the solvent diffusion method, had a functional hydrophilic surface for stability in water, and was able to encapsulate a large number of hydrophobic drugs within its highly branched polymeric structure.[1]

In the interest of further developing this new type of monomer, the monomer was modified to include sulfur pendants within the polymer nano-cavities. This modification successfully allowed for the encapsulation of Bi-DOTA complexes, allowing for better X-ray contrast images while the previous HBPE was only able to encapsulate minimal amounts.[22] Another thought was to increase the amphiphilicity of this type of hyperbranched polyester to allow for the encapsulation of more hydrophilic drugs and dyes. For this project, it was decided to copolymerize the diacid monomer with diethylene glycol or triethylene glycol to introduce hydrophilic oxygens into the polymer backbone to make a pseudo-branched polyester (PBPE) copolymer. These polymers were designed to be used for the encapsulation and delivery of therapeutic molecules for the treatment of LNCaP prostate cancer cells.

Polymeric Nanoparticles: A Tool for Cancer Treatment

The encapsulation and targeted delivery of anti-cancer drugs is important to the health of the patient. Systemic dosages of these cytotoxic drugs cause horrible side effects including but not limited to: pain, nausea, vomiting, constipation, and hair loss. Furthermore, free, non-encapsulated drug can interact with healthy cells causing cell death to healthy cells as well as cancer cells. Thus, nanoparticles are versatile, powerful tools that can be modified for the encapsulation of therapeutic molecules to be selectively delivered to cancer cells through surface
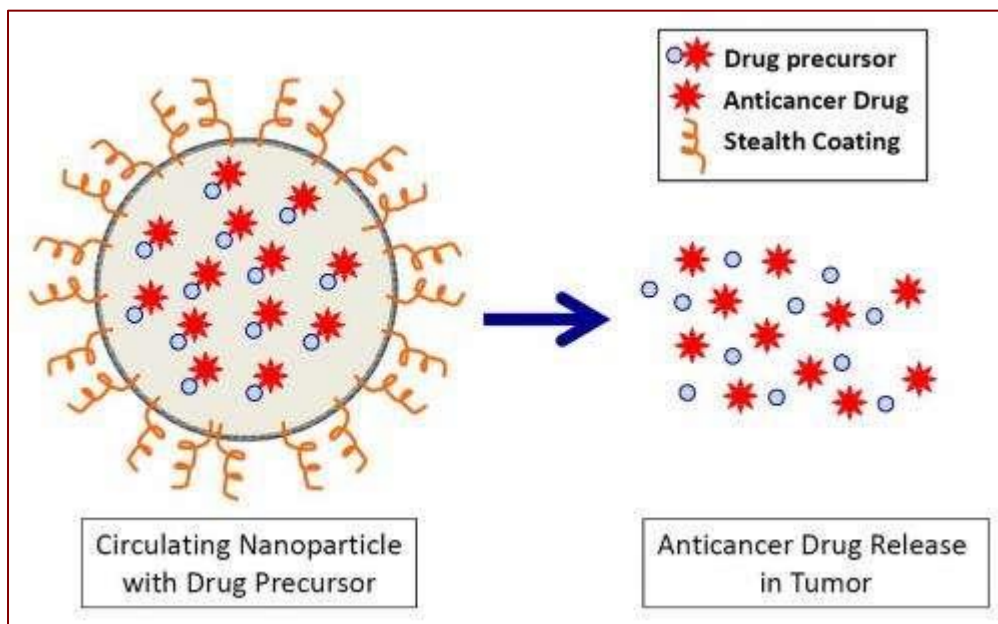
Figure 2: General structure of a polymeric nanoparticle loaded with a therapeutic cargo.[23]

modification with a targeting ligand. Their three-dimensional shape, chemical composition, and surface functionality can all be changed and fine-tuned for specific targets and uses.[24] With a targeting ligand attached, the nanoparticles will have a strong affinity for receptors on the surface of the targeted cancer cell, will be taken in through endocytosis, and broken down by the acidic and redox conditions of the cancer cell microenvironment, releasing its therapeutic cargo to the cancer cell.[25,26]

Determining whether or not a nanoparticle was successfully modified with a targeting molecule and loaded with its therapeutic cargo can be done with the help of different cytotoxicity and internalization assays.[27-29] For the assays presented in these publications, controls show no cytotoxicity while only the targeting ligand-labeled nanoparticle will cause cytotoxicity to the cancer cells. The MTT (3-(4,5-dimethylthiazol-2-yl)-2,5-diphenyltetrazolium bromide) assay tests cytotoxicity of compounds to a cell line. It represents cytotoxicity as percent cell viability through the amount of fluorescence intensity of formazan, which is reduced by mitochondrial reductase in live cells. If the cells survived the treatment, then there will be an absorbance between 500 –

600 nm correlating to formazan. Controls will result in maximum fluorescence which shows 100

percent cell viability. The positive control will give the baseline fluorescence showing 0 percent

cell viability.[30]

Chapter III

Results and Discussion

Polymer Synthesis and Characterization

Synthesis: Our first generation HBPE polymer was able to encapsulate hydrophobic drugs and dyes due to the hydrophobic nanocavities present inside the polymer.[1] In order to increase loading efficiency and allow for the encapsulation of hydrophilic drugs and dyes, we synthesized more amphiphilic HBPE polymers by introducing either diethylene glycol or triethylene glycol into the polymer backbone. This was done via a co-condensation in the melt condition catalyzed by p-tolulenesulfonic acid (pTSA). The synthesis of these two polymers, dubbed pseudo-branched polyester (PBPE) polymer, is demonstrated in **Scheme 1**. We first synthesized 4-bromobutyl acetate (**2**) by reacting tetrahydrofuran (THF) with potassium bromide and acetyl chloride in acetonitrile. The resulting compound (**2**) was characterized by NMR spectroscopy. To synthesize the trifunctional diester (**3**), diethyl malonate (**1**) is reacted with 4-bromobutyl acetate (**2**) in a polar aprotic solvent using a weak base. The trifunctional diester (**3**) obtained was purified and characterized by NMR spectroscopy. We then made the trifunctional diacid (**4**) through a base hydrolysis of the synthesized trifunctional diester (**3**), and then back titrated using hydrochloric acid. The trifunctional A_2B monomer (**4**) was purified using column chromatography and characterized by NMR and FT-IR spectroscopic methods. To synthesize the first PBPE polymer (**7**,
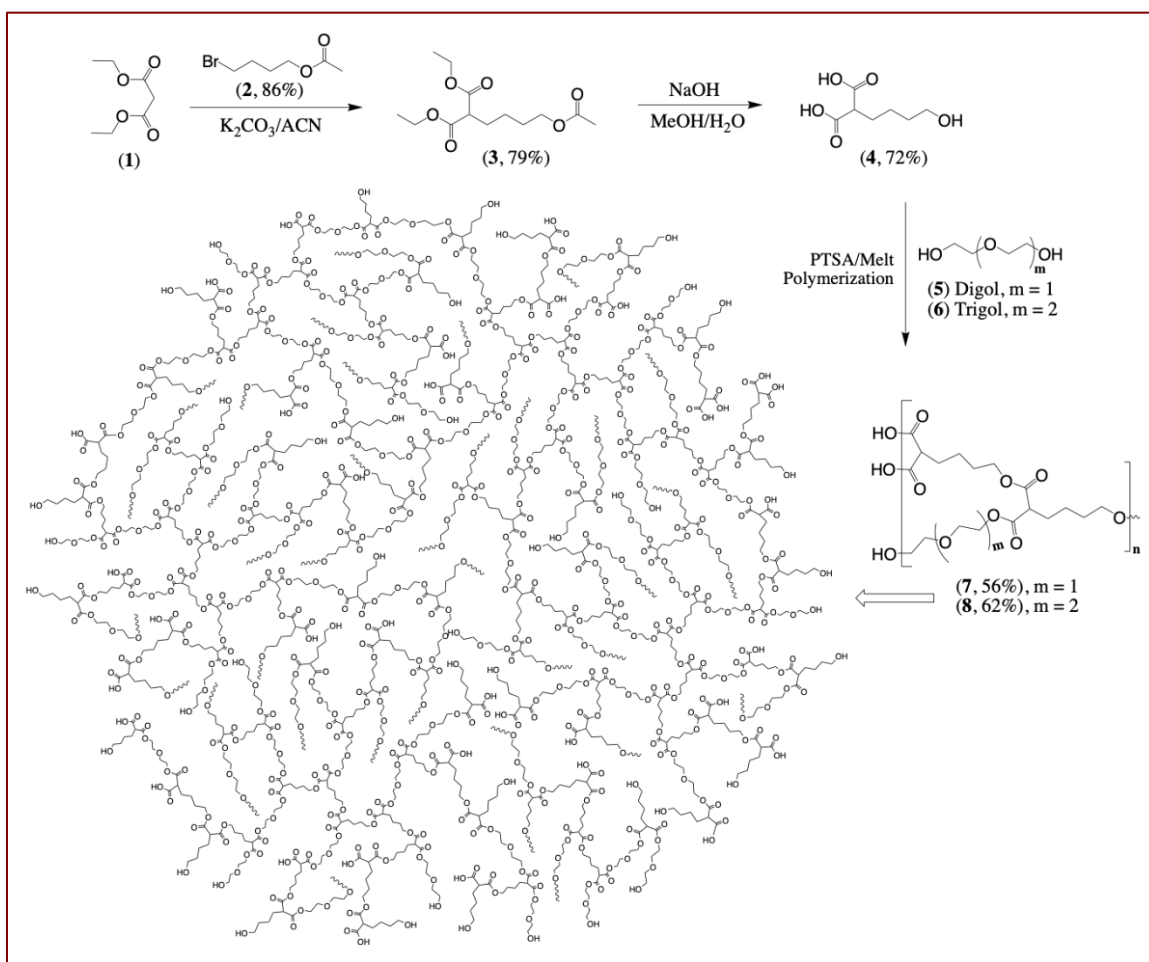
Scheme 1: Synthesis of our new pseudo-branched polyester (PBPE) polymers (7, 8) from a proprietary A₂B monomer (4) and diethylene glycol (5) or triethylene glycol (6).

Scheme 1) the previously synthesized A$_2$B monomer (**4**) and diethylene glycol (**5**) were used in a

1:1 molar ratio with a catalytic amount (100:1) of pTSA. The second PBPE polymer (**8**, **Scheme 1**)

was synthesized by substituting diethylene glycol (**5**) in the previous reaction with triethylene

glycol (**6**) using the same molar equivalents and catalyst concentration. For both reactions, to a 5

mL round bottom flask (RBF) the A$_2$B monomer (**4**) and diethylene glycol (**5**) or triethylene glycol

(**6**) were premixed, degassed to remove dissolved oxygen and water, and put under an ultra-high

purity (UHP) nitrogen blanket. Freshly recrystallized catalyst pTSA in a catalytic amount (1:100)

was then added. After purging the RBF, a steady flow of UHP-nitrogen gas was flown over the

reaction and the RBF was subsequently lowered into the oil bath. Stirring was introduced and the

reaction was heated up to 140 ºC for 8 hours to allow for the formation of oligomers. At this point, medium vacuum (1.5 mm/Hg) was introduced to the reaction removing most of the water generated. After 30 minutes, high vacuum ($4x10^{-4}$ mm/Hg) was introduced and the sample was allowed to continue polymerization for 12 hours. The two synthesized PBPE polymers (**7**, **8**) were purified using a mixed solvent precipitation method where a concentrated solution of polymer in methanol was made, precipitated in de-ionized water, and collected via centrifugation. The samples were dried in a vacuum oven overnight, resulting in pure polymers. Both the purified digol co-polymer (**7**) and trigol co-polymer (**8**) were highly viscous, amber in color, and soluble in methanol, dimethyl sulfoxide (DMSO), dimethyl formamide (DMF), tetrahydrofuran, and chloroform. This solubility data indicates the successful incorporation of diethylene glycol (**5**) or triethylene glycol (**6**) into their respective polymer backbones (**7**, **8**) and is a large improvement over our first generation HBPE polymers, which were only soluble in DMF and DMSO. [1] The resulting polymers were characterized using various spectroscopic methods and are described below.

FT-IR, TGA, and DSC: There are several characteristic, strong peaks observed in the FT-IR spectra of these two polymers (**Figure 3A – B**) shown in grey for the digol co-polymer and green for the trigol co-polymer. The strong peak at 1730 cm^{-1} for both polymers represents the ester carbonyl groups (C=O). The shift of this peak from 1714 cm^{-1} of the carbonyl group of a carboxylic acid in the A_2B monomer (**4**) (blue) suggests that polymerization was successful. This was again confirmed by the ester group at 1165 cm^{-1} from C-O stretching and also at 1126 cm^{-1} representing the repeating ether groups present in the diols. The peaks from $2970 – 2800$ cm^{-1} represent CH_2 stretching which is expected due to the aliphatic segment in the A_2B monomer. TGA results shown in **Figure 3C** shows both polymer samples had a 10% weight loss around 265 ºC, indicative of ester degradation. The trigol co-polymer (**8**) has a slightly higher degradation
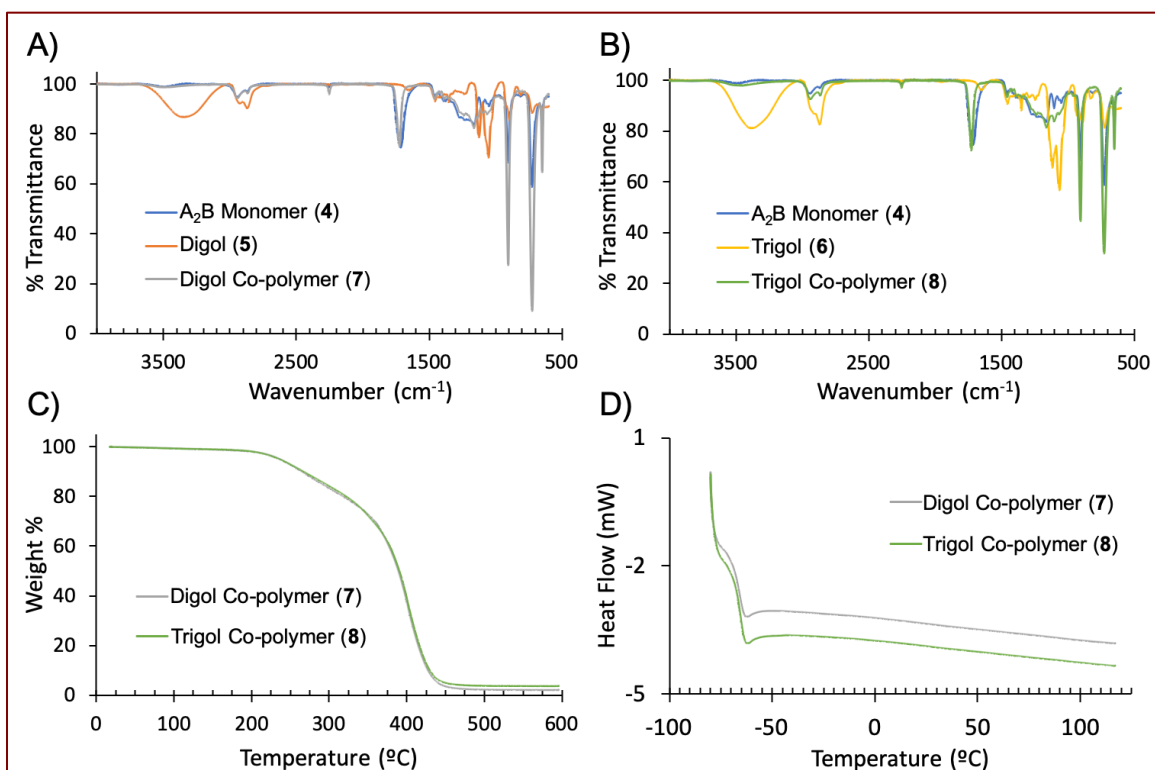
Figure 3: A) FT-IR spectra of the monomers: A_2B monomer (*4*), diethylene glycol (*5*), and subsequent PBPE copolymer (*7*); B) FT-IR spectra of the monomers: A_2B monomer (*4*), triethylene glycol (*6*), and subsequent PBPE co-polymer (*8*); C) Stacked TGA chromatograms of digol PBPE copolymer (*7*) and trigol PBPE copolymer (*8*); D) DSC curve overlay of digol PBPE co-polymer (*7*) and trigol PBPE copolymer (*8*).

temperature than the digol co-polymer (**7**) which can be attributed to the additional ether group in triethylene glycol. The results show the polymer will remain thermodynamically stable at biological temperatures (37 ºC). Results from DSC (**Figure 3D**) showed both polymer samples (**7, 8**) have glass transition temperatures (T_g) at approximately -66ºC and displayed no crystallization (T_c) or melting (T_m) peaks. This suggests that both polymers are 100% amorphous, attributed to the flexibility of the ether linkages in the polymer backbone.

¹H NMR: ¹H NMR spectra of the A_2B monomer, diethylene glycol, and the resulting polymer are shown in **Figure 4**. The representative peaks in the A_2B monomer spectrum for the six central aliphatic protons (**4**; peaks 2 – 4) from 1.2 – 1.8 ppm can be seen in the digol co-polymer with a slight chemical shift downfield from 1.3 – 2.4 ppm (**7**; peaks 6 – 8). The single proton between the two carbonyl groups (**4**; peak 1) and the two protons with a hydroxyl

neighbor (**4**; peak 5) at 3.2 and 3.4 ppm respectively are seen in the polymer with a downfield

shift at 3.6 ppm (**7**; peak 5) and 4.0 ppm (**7**; peak 9) respectively. In the spectrum for diethylene

glycol, the representative peaks for the four amphiphilic protons (**5**; peak 2) and the four protons

with a hydroxyl neighbor (**5**; peak 1) at 3.6 and 3.7 ppm respectively can also be seen in the digol

co-polymer spectrum with a slight chemical shift downfield, observed from 3.7 – 4.2 ppm (**7**;

peaks 1 – 3). The peak for the two protons with a carboxyl neighbor (**7**; peak 4) in the digol co-

polymer spectrum have a chemical shift of 4.3 ppm. For the ^{1}H NMR spectrum of the trigol co-

polymer seen in **Figure 5**, the chemical shifts of the six aliphatic protons (**8**; peaks 6 – 8), the

single proton between the two carbonyl groups (**8**; peak 5), and the two protons with a hydroxyl

neighbor (**8**; peak 9) are very similar to the chemical shifts of the same chemical groups in the

digol co-polymer (**7**, **Figure 4**). The same can be said for the representative peaks of the eight

amphiphilic protons (**8**; peaks 2 – 3) and the two protons with a hydroxyl neighbor (**8**; peak 1) in

the triethylene glycol monomeric unit, with the difference being there are four more amphiphilic

protons (**Figure 5**, 3.65 ppm) in triethylene glycol unit vs the diethylene glycol unit in the digol co-

polymer (**7**).

Due to the nature of polymers in that they are made up of many repeat units, protons on

the same repeat unit in different locations within the polymer are in a slightly different chemical

environment. This phenomenon is observed in the ^{1}H NMR spectra of both the digol and trigol

co-polymers exhibited by the broad, irregular polymer peaks and the slight downfield shift. This

peak broadening can cause signals to overlap and make them difficult to isolate and identify in

contrast to the spectra of small molecules, which tend to exhibit more defined sharp peaks.

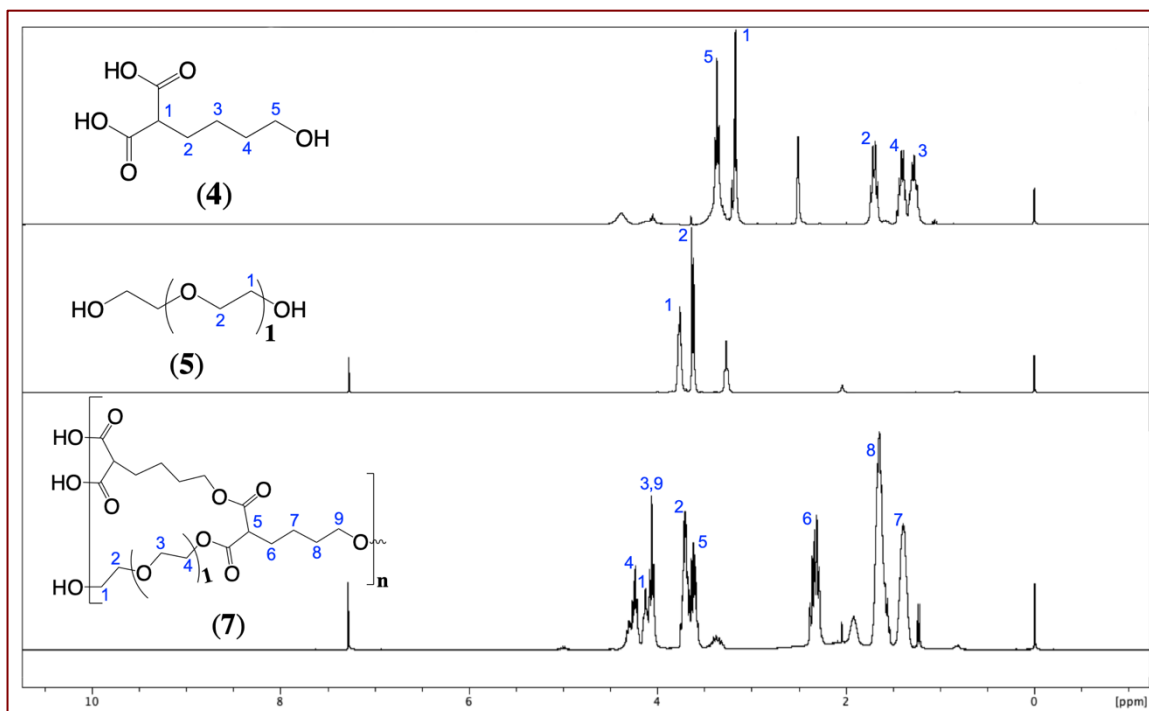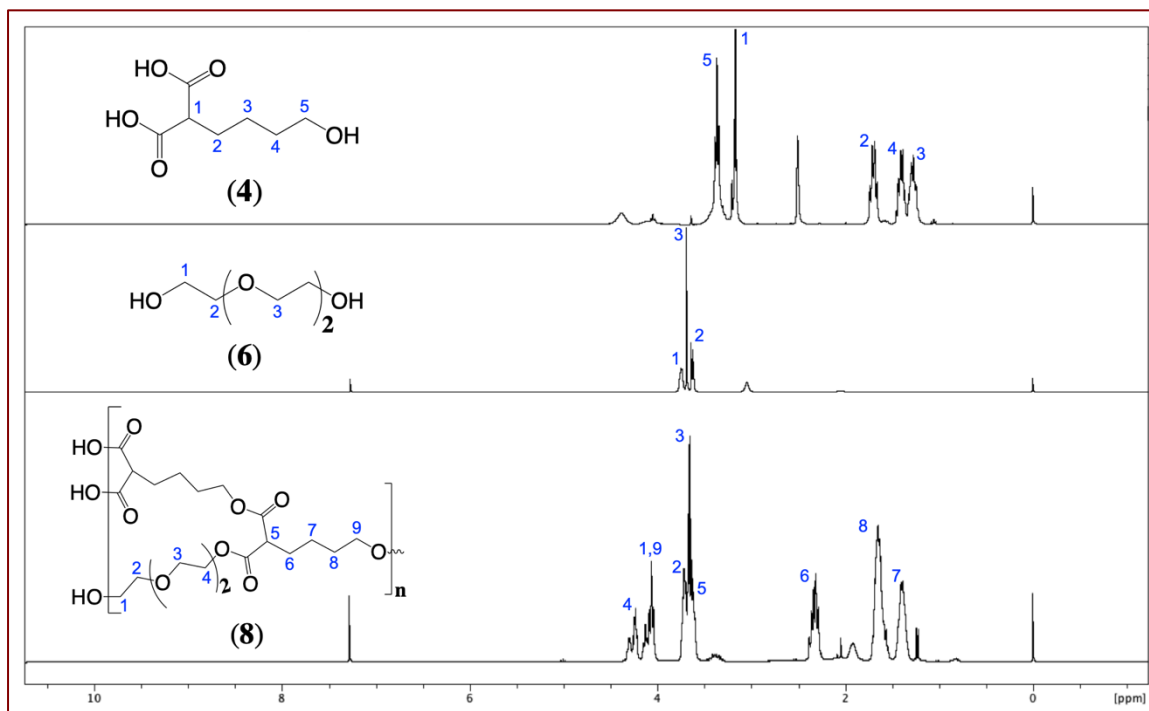**Figure 4**: ^1H NMR spectra of the monomers: A_2B monomer (**4**), diethylene glycol (**5**), and subsequent PBPE co-polymer (**7**).

Figure 5: ^1H NMR spectra of the monomers: A_2B monomer (**4**), triethylene glycol (**6**), and subsequent PBPE co-polymer (**8**).

¹³C NMR: In the ¹³C NMR spectrum of the digol co-polymer shown in **Figure 6**, the peak at approximately 174 ppm represents a carbonyl carbon of free carboxylic acid groups in the polymer (**7**; peak 6), while the peak at approximately 169 ppm represents carbonyl carbons of esters (**7**; peak 5) located in the polymer backbone. The peaks at 69.0 and 72.5 ppm in the digol co-polymer spectra (**7**; peaks 2 – 3) represent the amphiphilic carbons (**5**; peak 2) in diethylene glycol monomeric unit. The peak at 64.2 ppm represents the carbon attached to an ester (**7**; peak 4). The peaks at 62.5 and 61.7 ppm represent carbons with a hydroxyl neighbor in the aliphatic region of the backbone (**7**; peak 11) and carbons with a hydroxyl neighbor in the amphiphilic region of the backbone (**7**; peak 1). The peaks at 63.4 ppm correspond to the carbons attached to an ester from the A_2B monomer self-condensation. The peak at 51.8 ppm represents the carbon that has two carbonyl neighbors (**7**; peak 7). The peaks from 34.3 – 23.5 ppm represent the central aliphatic carbons (**7**; peaks 8 – 10) of the A_2B monomeric unit. The ¹³C NMR spectrum of the trigol co-polymer (**8**) (**Figure 7**) is highly similar to the spectrum of the digol co-polymer (**7**)
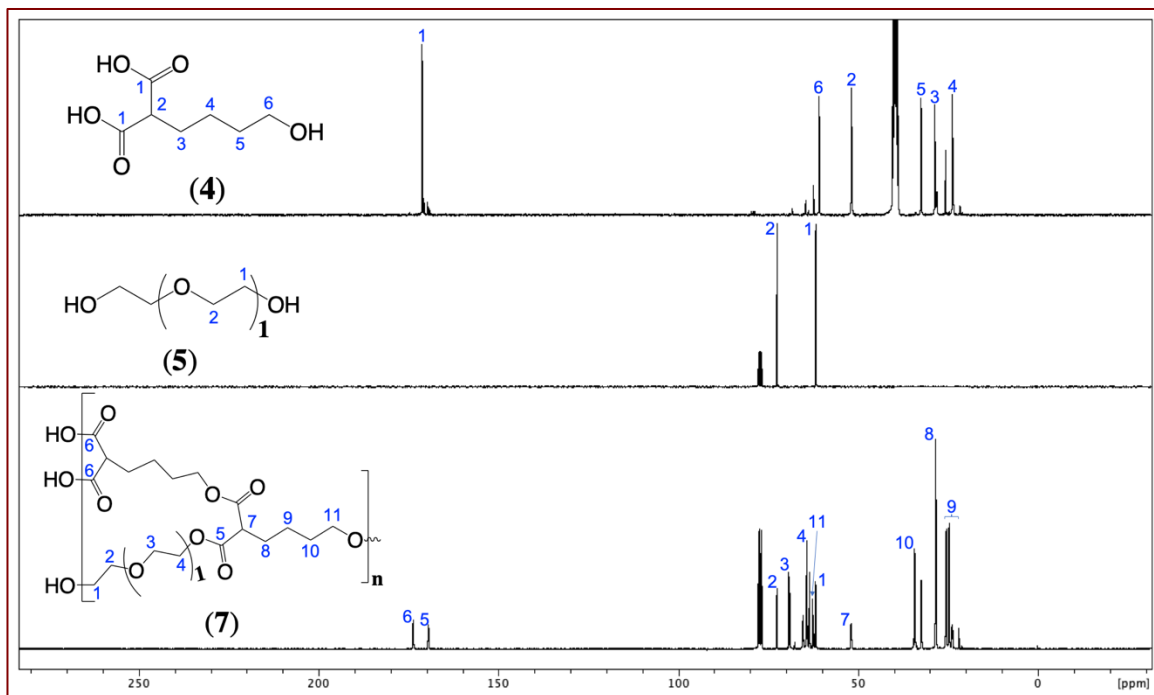

Figure 6: *¹³C NMR spectra of the monomers: A_2B monomer (**4**), diethylene glycol (**5**), and subsequent PBPE co-polymer (**7**).*

18
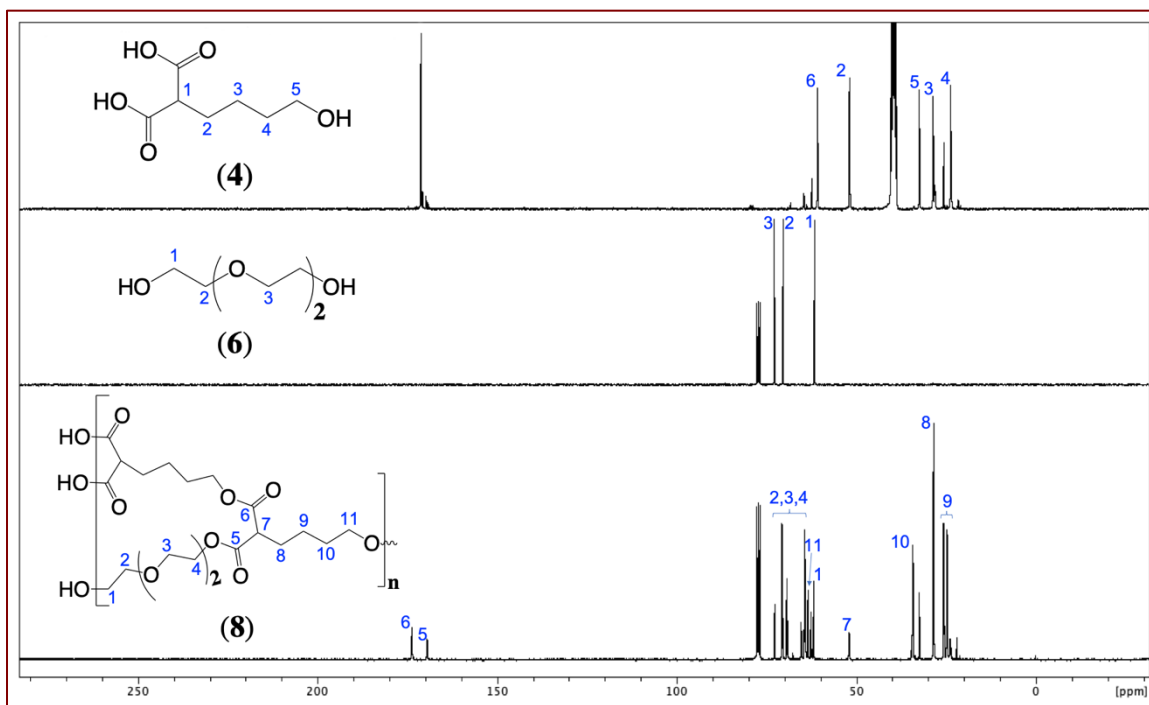
Figure 7: *^{13}C NMR spectra of the monomers: A$_2$B monomer (**4**), triethylene glycol (**6**), and subsequent PBPE co-polymer (**8**).*

with one difference: the peak at 70.5 ppm in the trigol co-polymer spectrum represents two carbons (**6**; peaks 2 and 4) present in triethylene glycol (**6**) but not present in diethylene glycol (**5**).

MALDI-TOF and GPC: MALDI-TOF spectra (**Figure 8A**) obtained from the digol co-polymer (**7**) had a large fragment with an m/z value of 29,643 and spectra obtained from the trigol co-polymer (**8**) had a large fragment with an m/z value of 33,996. Both PBPE polymers exhibited high molecular weights, large enough for use as a drug delivery system. GPC chromatograms (**Figure 8B**) showed both the digol and trigol co-polymers (**7**, **8**) were successfully synthesized with high molecular weight product being eluted between 31 and 32 minutes. The trigol co-polymer eluted slightly after the digol co-polymer, but the trigol co-polymer peaked at a higher molecular weight. In GPC, larger molecules elute first and both polymers were subjected to the same reaction time,

so the previous statement can be explained by triethylene glycol being a longer "chain-extender" than diethylene glycol.

Figure 8: A) Stacked MALDI-TOF chromatograms of digol PBPE copolymer (**7**) and digol PBPE copolymer (**8**); B) GPC chromatograms of digol PBPE copolymer (**7**) and trigol PBPE copolymer (**8**).
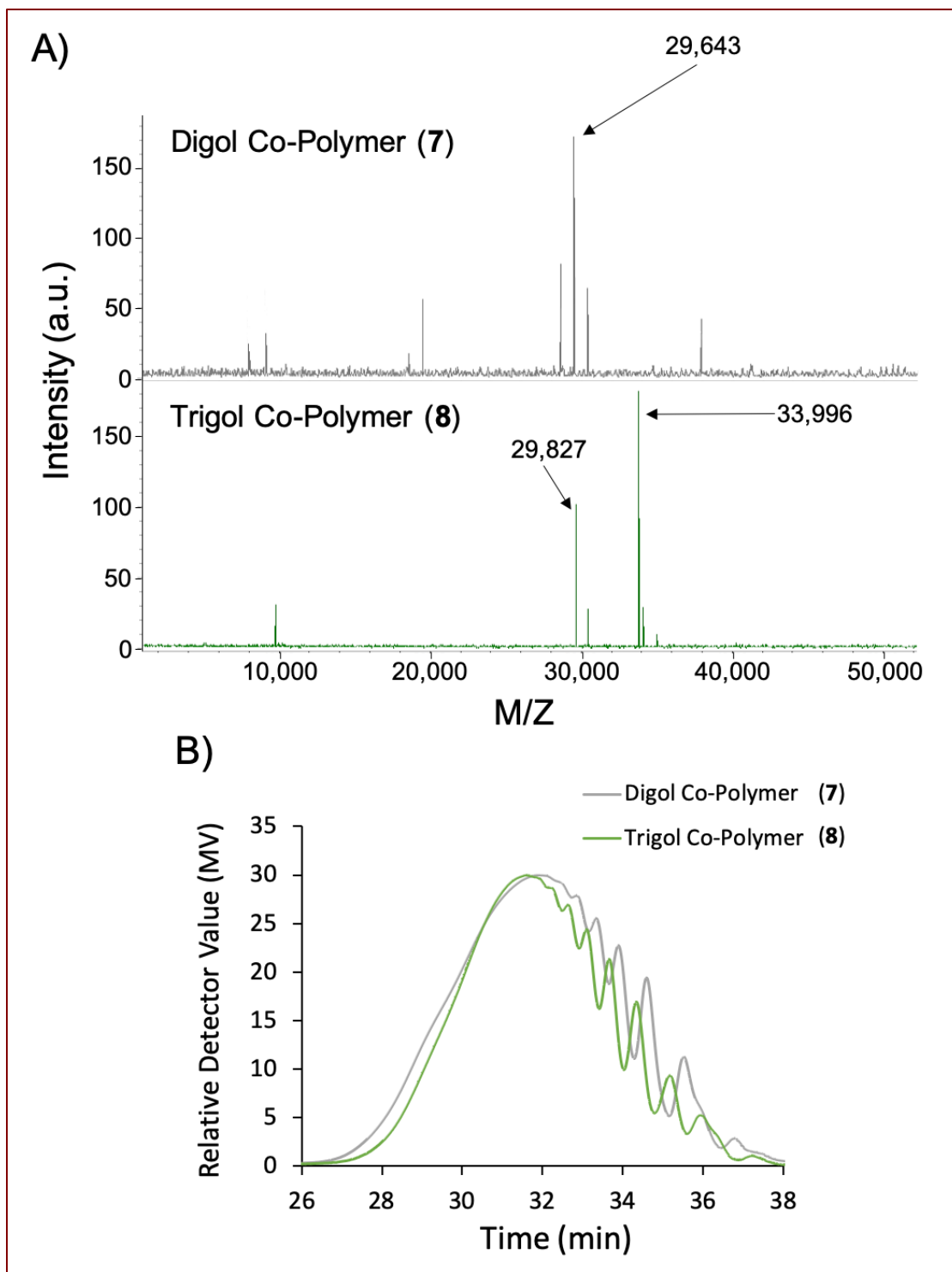
Polymeric Nanoparticle Synthesis and Characterization

Synthesis: After all polymer characterization techniques were completed, the trigol PBPE copolymer (**8**) was transformed into polymeric nanoparticles (**10**) for drug encapsulation using the solvent diffusion method and EDC/NHS chemistries according to **Scheme 2**. For the encapsulation of doxorubicin, the trigol PBPE copolymer (30 mg) and doxorubicin (6 µL, 5 µg/µL) were dissolved in 300 µL of DMSO, mixed, added dropwise to DI water (4 mL) and mixed again. This resulted in the formation of our doxorubicin-loaded PBPE nanoparticles (**9**). Dispersion in water forces the hydrophobic moieties of our PBPE polymer to aggregate and align with each other, exposing the hydrophilic segments to the aqueous environment which are stabilized by hydrogen bonding between surface carboxylic acid and hydroxyl groups. The doxorubicin is forced to order within the amphiphilic regions of the PBPE polymer, resulting in the formation of carboxylic acid functionalized, doxorubicin-encapsulating, globular polymeric nanoparticles. It is essential to note that our polymeric nanoparticles are capable of encapsulating and delivering both hydrophobic and hydrophilic theranostic molecules as well, due to the amphiphilic nature of the polymeric cavities. Our PBPE nanoparticles will need to be functionalized with a targeting ligand if they are to be internalized by cancer cells. In this case, we aim to target PMSA+ LNCaP prostate cancer cells so we have chosen folate to use as our targeting ligand, as it has a high
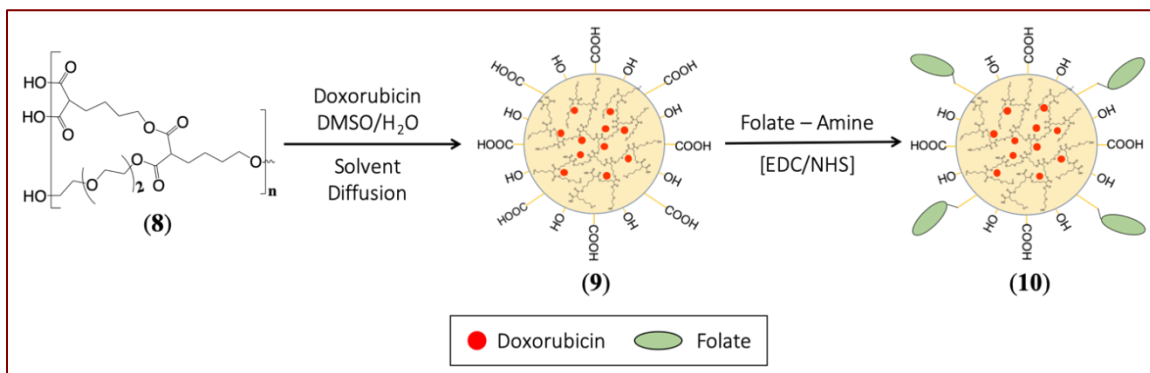
Scheme 2: *Synthesis of PBPE nanoparticles and ligand surface modification.*

affinity for the PMSA receptor. We prepared for the conjugation of folic acid to the surface of our drug-loaded PBPE nanoparticles (**9**) using previously synthesized aminated folic acid.[31] This is easily achieved through EDC/NHS chemistries. After conjugation, our drug-loaded, folate functionalized PBPE nanoparticles (**10**) were purified via dialysis and characterized as discussed below.

DLS, Zeta Potential, and Fluorescence: To determine the size of our PBPE nanoparticles, they were subjected to dynamic light scattering (DLS). **Figure 9A** shows our unconjugated PBPE nanoparticles (**9**) have an average size of approximately 74 nm, and then an average size of 79 nm after conjugation with folic acid (**10**). These nanoparticles are an appropriate size for use as a drug delivery system as particles over 500 nm are not easily internalized in cells. Determining the surface charge of our PBPE nanoparticles uses a technique that measures the potential difference between the nanoparticle surface and the conducting liquid they are suspended in, known as zeta potential. The surface charge of our unconjugated (**9**) and conjugated (**10**) PBPE nanoparticles was measured (**Figure 9B**) and we found that before conjugation the nanoparticles have a surface charge of approximately -30 mV which is indicative of a carboxylic acid functional surface and expected since carboxylic acids have an overall negative charge. After conjugation, zeta potential was measured and found to be approximately -36 mV. This change in zeta potential confirms the successful modification of our PBPE nanoparticle with folate. It is also important to note that this surface charge has a large contribution to our PBPE nanoparticles' stability in water. Fluorescence of the PBPE nanoparticles was also measured after encapsulation with doxorubicin and conjugation with folic acid (**Figure 9C – D**). Fluorescence emission spectra revealed peaks at 350 nm and 595 nm, correlating to folic acid (**Figure 9C**) and doxorubicin (**Figure**
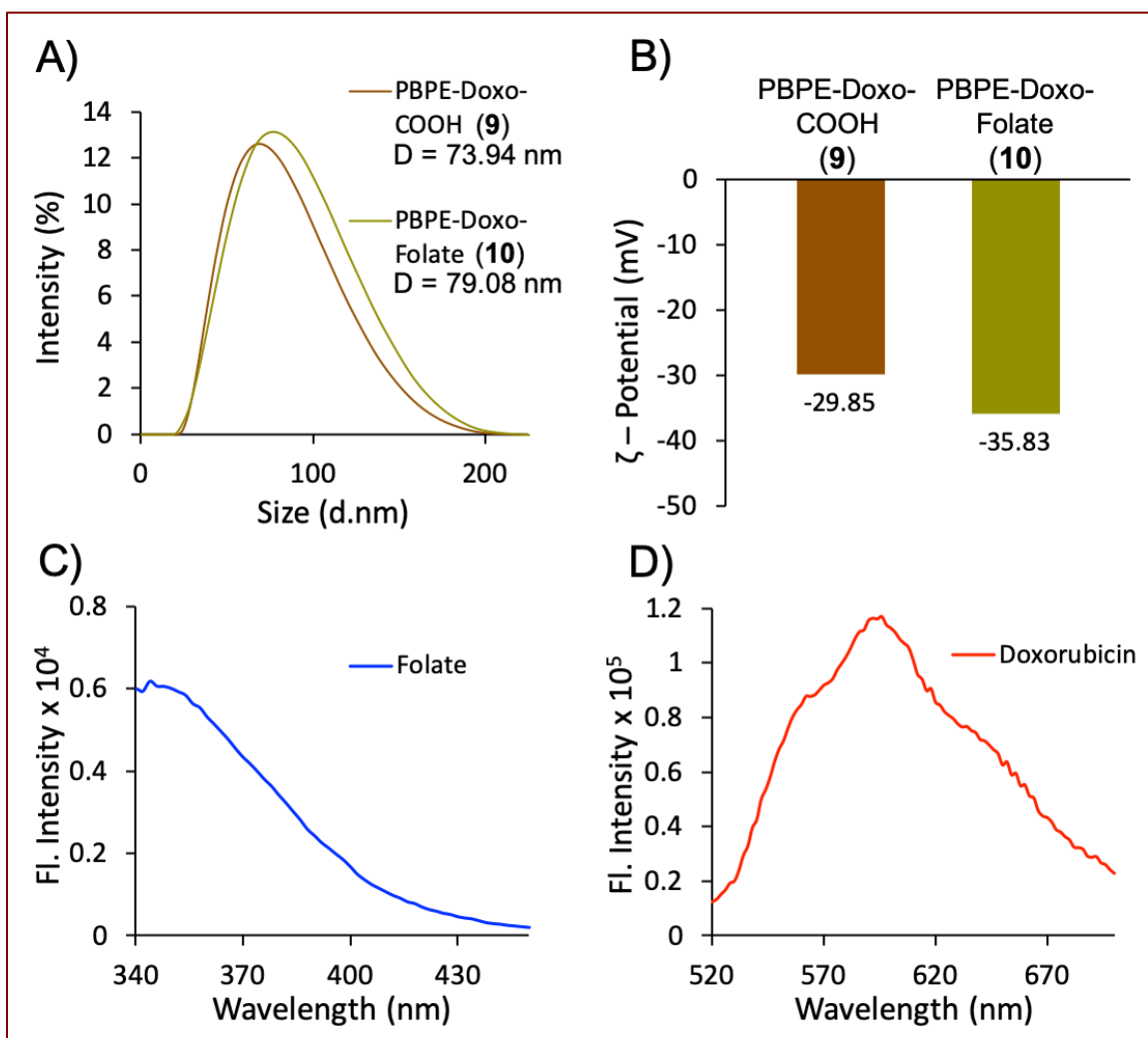
Figure 9: A) DLS curves of the trigol PBPE nanoparticle before (9) and after (10) conjugation with the targeting ligand folic acid; B) ζ – Potential of the trigol PBPE nanoparticle before (9) and after (10) conjugation with the targeting ligand folic acid; Fluorescence spectra for the folate (C) conjugated, doxorubicin (D) loaded nanoparticle (10).

9D) emission, respectively. This showed that folate was successfully conjugated to the PBPE nanoparticles' surfaces. It also revealed that doxorubicin was successfully encapsulated and maintains its fluorescence activity within the polymer matrix and the nanoparticles can be tracked during cellular internalization in real time via fluorescence imaging.

Cell Culturing, Cytotoxicity, and Internalization

23

MTT Assay: To determine the efficacy of our PBPE-based nanomedicine, an MTT assay was used on LNCaP cells and PC3 cells (as a control) after incubation with the PBPE nanoparticles. LNCaP prostate cancer cells and PC3 cells were cultured in 96-well plates 24 h before the assay was to be conducted. The cells were then incubated with PBPE-Doxo-COOH (**9**) and PBPE-Doxo-Folate (**10**) with a well left untreated to be used as a control for 48 h in a humidified incubator at 37 ºC at 5% CO_2 and results were taken at 24 and 48 hours. After incubation, both cell lines were treated with MTT/Phosphate-buffered saline (PBS) solution and incubated for an additional 4-6 hours. The efficacy of our PBPE-based nanomedicine was determined by measuring the fluorescence intensity of formazan at 560 nm. MTT is metabolized by healthy cells to formazan, meaning higher intensity gives more cell viability. The results are detailed above in **Figure 10**. Following **Figure 10A**, the assay showed the folate-functionalized, doxorubicin-encapsulating nanoparticles (**10**) were highly toxic to the LNCaP cells (PMSA+), showing approximately 40% cell viability after only 24 h of incubation. Viability was even lower after 48 h of incubation, showing approximately 80% cell death. Unconjugated PBPE nanoparticles showed negligible reductions in cell viability over the control. **Figure 10B** indicates the folate-functionalized, doxorubicin-

encapsulating nanoparticles are not very toxic to the PC3 cells (PMSA-) (84% cell viability after 48

h of incubation). These results suggest our folate-functionalized, doxorubicin-carrying PBPE

nanoparticles (**10**) were internalized, degraded, and released their cytotoxic payload in the

cytosol, initiating apoptosis. The results also indicate the PBPE-Doxo-Folate nanoparticles (**10**) are

highly selective to the LNCaP prostate cancer cell line (PMSA+) over the PC3 cell line (PMSA-). This

is due to PC3 cells having a normal expression of the PMSA receptor.

Cellular Internalization: The LNCaP cell line was incubated for 24 h in petri dishes with

PBPE-Doxo-COOH (**9**) and PBPE-Doxo-Folate (**10**), along with a control sample with no treatment.
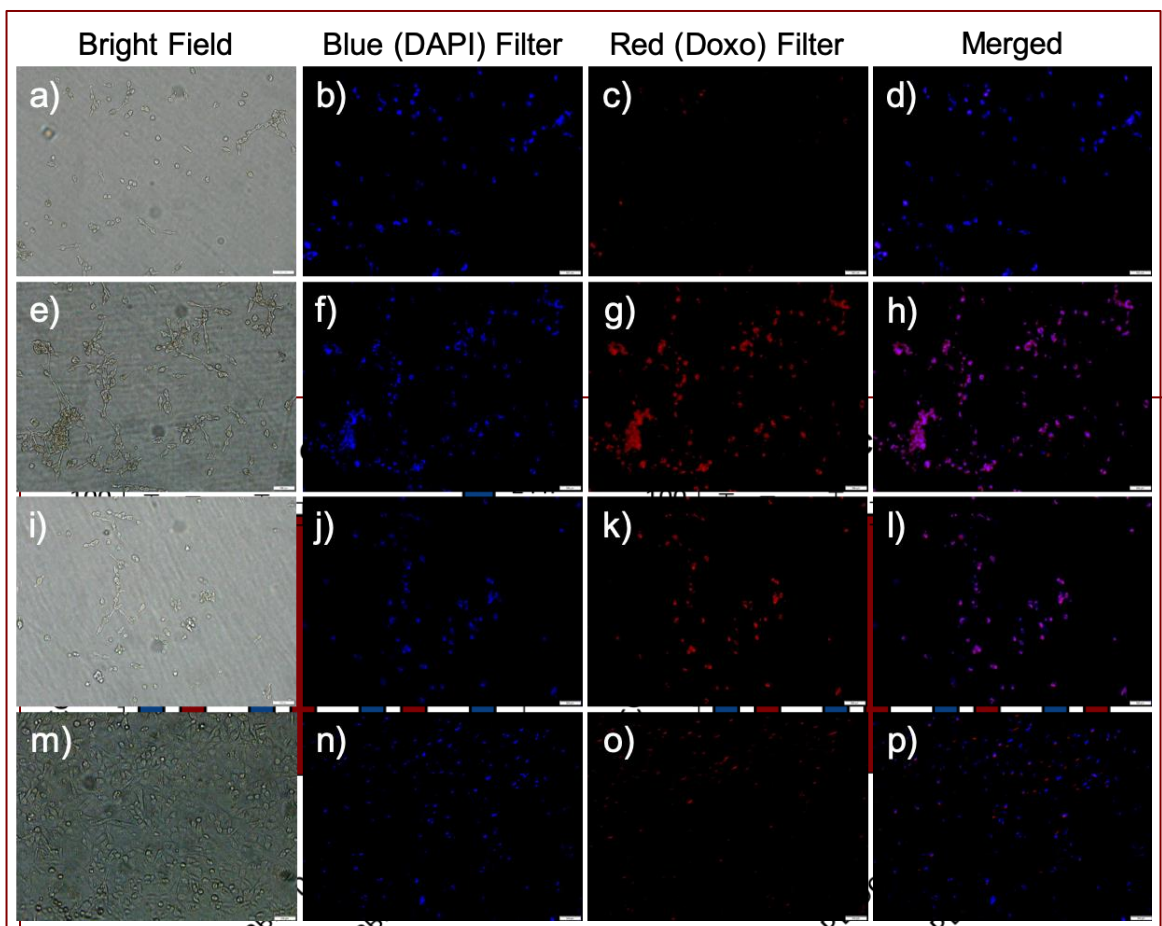
Figure 11: *a-d) No or minimal internalization of PBPE-Doxo-COOH (**9**) was observed in LNCaP cells (scale bar 500 µm). e-h) Internalization of PBPE-Doxo-Folate (**10**) was observed after 12 h due to the folate-receptor-mediated endocytosis. i-l) Cell death is observed within 24 h when PBPE-Doxo-Folate (**10**) is incubated with LNCaP cells. m-p) Minimal internalization of PBPE-Doxo-Folate (**10**) was observed in PC3 cells. Nuclei stained with DAPI (blue).*

One sample was also incubated with PBPE-Doxo-Folate (**10**) for 48 h, to track PNP internalization via doxorubicin fluorescence emission at 600 nm. Both the treated and control plates were analyzed under a fluorescence microscope and the results are shown below in **Figure 11a – p**. The images confirm that the PBPE-Doxo-Folate (**10**) nanoparticles were successfully internalized, and nanoparticles lacking the folate targeting ligand (**9**) had minimal internalization.

Determination of Cytosolic ROS Stress: We hypothesized that LNCaP cells were generating cytosolic reactive oxygen species (ROS) after incubation with our PBPE-Doxo-Folate (**10**) nanoparticles. To determine the level of ROS generation, we used Dihydroethidium (DHE, 32 μM) dye to track ROS in the cytoplasm. Fluorescence was captured from the cell culture dishes (**Figure 12A**) and the fluorescence was quantified using the ImageJ software (**Figure 12B**). Results indicated once doxorubicin was released into the cytoplasm, substantial amounts of ROS were generated in the cytoplasm. This is due to fact that doxorubicin binds to cytosolic DNA, producing ROS as shown in **Figure 12A**. There is minimal ROS generated in cells incubated with PBPE-Doxo-COOH (**9**) nanoparticles due to the lack of the targeting ligand folate on the nanoparticles' surfaces. To further confirm that the ROS generation was due to the cytotoxicity of our folate-conjugated, drug-loaded nanomedicine and the potential reason for cell death, another experiment was done in the presence of hydrogen peroxide (H_2O_2, 3.0 mM). Results showed the amount of ROS generation was validated, showing similar results to the MTT assay performed earlier. In all, these experiments indicated ROS species are generated in LNCaP cancer cells when incubated with PBPE-Doxo-Folate nanoparticles, ultimately causing cell death.
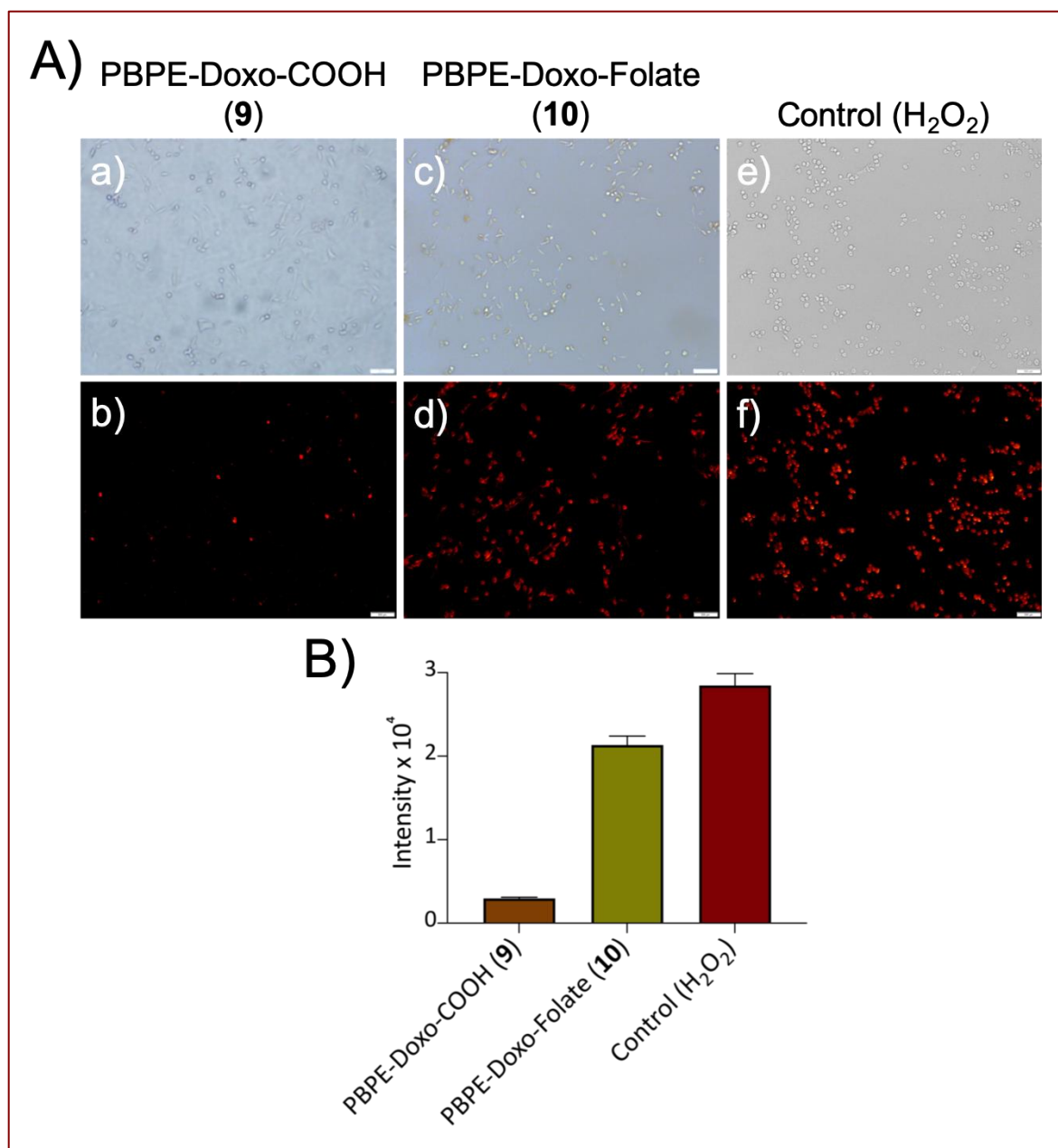
Figure 12: Determination and quantification of ROS in LNCaP cells (scale bar 500 µm). Aa-b) Generation of cytoplasmic ROS in the presence of PBPE-Doxo-COOH (9), which are labelled using DHE dye. Presence of NAC (3.0 mM) inhibits the ROS generation. B) The amount of ROS generation was quantified directly from the corresponding fluorescence microscopic images using ImageJ software.

Comet Assay and Migration Assay: A comet assay was performed (**Figure 13A – B**) to study

the level of DNA damage done to the LNCaP cell line when treated with folate-conjugated,

doxorubicin-encapsulating PBPE nanoparticles (**10**). Results indicated the unconjugated,

doxorubicin-encapsulating PBPE nanoparticles (**9**) gave minimal DNA damage, as there are no

tailing or olive shaped cells (**Figure 13A**). However, folate-conjugated, doxorubicin-encapsulating PBPE nanoparticles (**10**) showed a significant level of DNA damage, exhibited by the tailing and olive shaped cells (**Figure 13B**). Results showed our PBPE-Doxo-Folate nanoparticles (**10**) were effective in causing DNA damage to the LNCaP cancer cell line. A transwell migration assay was conducted to determine if our folate-conjugated, doxorubicin-encapsulating PBPE nanoparticles (**10**) are able to arrest the metastatic activity of LNCaP cancer cells. Starved LNCaP cells incubated with unconjugated, doxorubicin-encapsulating PBPE nanoparticles (**9**) showed a high level of metastatic activity, as these nanoparticles have no targeting ligand and thus were not internalized by the cancer cells. In another experiment, starved LNCaP cells were incubated with folate-
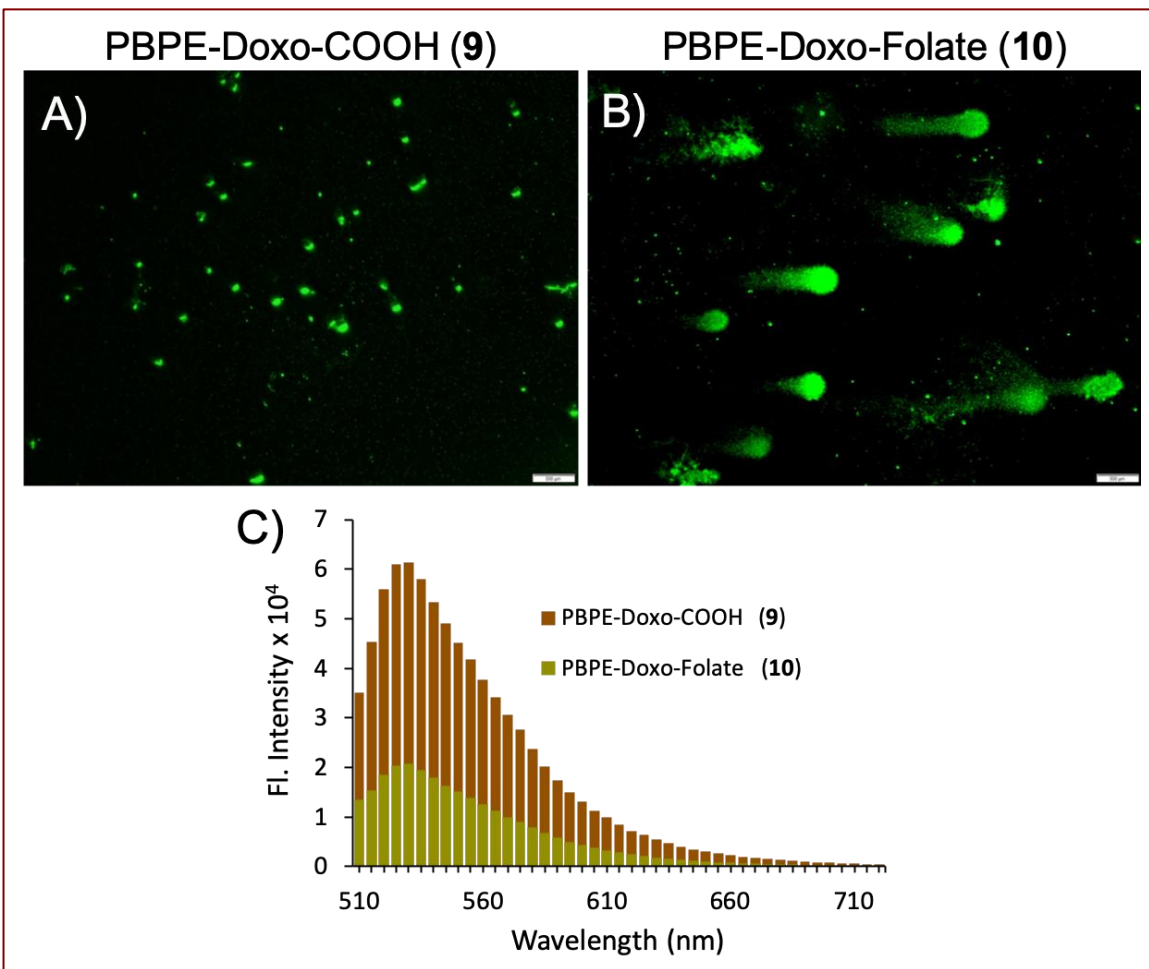
Figure 13: A) Control comet experiment using PBPE-Doxo-COOH (**9**) nanoparticles. B) Comet experiment using PBPE-Doxo-Folate (**10**) nanoparticles. Each experiment was performed in triplicate. C) Cell migration assay showing the effect of folate-conjugated, doxorubicin encapsulated nanoparticle therapy on the LNCaP cell migration process and to evaluate the anti-metastatic effect of the therapy.

conjugated, doxorubicin-encapsulating PBPE nanoparticles (**10**) showed a minimal level of

metastatic activity. The results shown in **Figure 13C** indicate our folate-conjugated, doxorubicin-

encapsulating PBPE nanoparticles (**10**) are effectively able to arrest the migration of the LNCaP

cancer cell line.

Chapter IV

Conclusions and Future Work

Hydrophilic, pseudo-branched polyester co-polymers were successfully synthesized from our proprietary A$_2$B monomer and diethylene glycol or triethylene glycol. Polymer characterizations showed polymers with high molecular weight, thermostability, and carboxylic acid functionality that allowed for further surface modification to attach targeting ligands. The PBPE polymer was successfully transformed to a PNP suspension, with PNPs having proper size for cellular internalization and surface-bound targeting ligands. The PNPs successfully encapsulated the anti-cancer drug doxorubicin while remaining stable at physiological conditions. Cytotoxicity and cell internalization studies showed the nanoparticle was successfully internalized by the LNCaP cancer cells and released its cytotoxic cargo, resulting in 80% cell death after 48 h of incubation.

Future work involves doing drug release studies on the PBPE nanoparticles to assess their loading efficiencies compared to our first-generation monomer HBPE and other nanoparticles. This is done by dialysis in the presence of esterase and under neutral and acidic pH, measuring the amount of doxorubicin fluorescence of the surrounding water before and after treatment. This will show their stability under those conditions and determine their loading and release efficiencies. In-vivo mice models that express prostate cancer are also considered for future work. The nanoparticles synthesized would have to be dramatically reduced in size due to the in-

vivo bio-incompatibility of large polymeric nanoparticles. Studies would need to be done to

determine if PBPE nanoparticles of such a small size are able to efficiently encapsulate its cargo.

Chapter V

Experimental Methods

<u>Materials</u>

Dimethylsulfoxide, acetonitrile, and diethyl malonate were obtained from Sigma Aldrich and used without further purification. Deuterated dimethyl sulfoxide (DMSO-d_6) and chloroform (CDCl$_3$) used in ^{1}H NMR and ^{13}C NMR spectroscopy were purchased from Cambridge Isotope Laboratories, Inc. 2,5-dihydroxybenzoic acid (DHB) matrix for MALDI-TOF mass spectroscopy was purchased from Bruker. The hydrophilic monomers (diethylene and triethylene glycol), the catalyst *p*-tolulenesulfonic acid (pTSA), 3-(4,5-dimethylthiazol-2-yl)-2,5-diphenyltetrazolium bromide (MTT), 4',6-diamidino-2-phenylindole (DAPI), ethylenediamine (EDA), N-hydroxysuccinimide (NHS), 1-Ethyl-3-[3-dimethylaminopropyl] carbodiimide hydrochloride (EDC), doxorubicin, trifluoroacetic acid (TFA), and regular solvents including tetrahydrofuran, hexane, and ethyl acetate were purchased from Fisher Scientific. The dialysis membrane (MWCO = 6-8K) was purchased from Spectrum Laboratories. Prostate specific membrane antigen negative (PSMA-) cells (PC3), and LNCaP (PSMA+) cells were obtained from American Type Culture Collection (ATCC). Cell culture media, serum, and antibiotics were purchased from Corning.

Synthetic Methods

Synthesis of 4-Bromobutyl Acetate (2): Tetrahydrofuran (12.2 mL, 148.4 mmol) and potassium bromide (21.1 g, 176.5 mmol) were added into a 250 mL round-bottom flask containing 150 mL of acetonitrile. The reaction mixture was cooled to 0 ºC, followed by dropwise addition of acetyl chloride (11 mL, 155.1 mmol). After which, the mixture was brought to room temperature, where it was continuously stirred for 36 h. Water was added to the reaction mixture and the product was then extracted with ethyl acetate. The organic layer was washed with water, dried over Na_2SO_4, and concentrated to obtain the pure product as a colorless liquid.

Yield: 24.3 g (85%). BP: >250 ºC. ^{1}H NMR (300 MHz, CDCl_3, δ ppm, J Hz): 1.79 (m, 2H), 1.92 (m, 2H), 2.03 (s, 3H), 3.46 (t, 2H, J = 7.6), 4.08 (t, 2H, J = 6.7). ^{13}C NMR (75 MHz, CDCl_3, δ ppm): 20.87, 27.36, 29.36, 33.03, 63.43, 170.95. IR (CHCl_3): 3038, 2926, 1352, 1243, 1052 cm^{-1}.[1]

Synthesis of 2-(4-Acetoxybutyl)malonic Acid Diethyl Ester (3): Diethyl malonate (1) (10 g, 62.5 mmol) and 4-bromobutyl acetate (2) (15.84 g, 81.3 mmol) were charged to a round-bottom flask with acetonitrile (120 mL) and stirred for 2 min at room temperature. [1] Then, potassium carbonate (34.5 g, 250.1 mmol) was added and refluxed for 36 h. Next, the mixture was filtered and the filtrate was concentrated to obtain a yellow liquid, extracted with ethyl acetate, and washed with water. The organic layers were combined and dried over Na_2SO_4, and purified by column chromatography using 4% ethyl acetate in petroleum ether as the eluent.

Yield: 13.02 g (76%). BP: 250 ºC. ^{1}H NMR (300 MHz, CDCl_3, δ ppm, J Hz): 1.28 (t, 6H, J = 7.6), 1.38 (m, 2H), 1.62 (q, 2H, J = 7.2), 1.98 (q, 2H, J = 7.7), 2.05 (s, 3H), 3.34 (t, 1H, J = 7.7), 4.09 (t, 2H, J = 6.6), 4.22 (q, 4H, J = 7.2). ^{13}C NMR (75 MHz, CDCl_3, δ ppm): 14.06, 20.79, 23.74, 28.25,

28.25, 51.84, 61.27, 63.89, 169.31, 171.11. IR (CHCl₃): 2982, 1728, 1463, 1367, 1233, 1151, 1029,

860 cm⁻¹.[1]

Synthesis of 2-(4-Hydroxybutyl)malonic Acid (4): 2-(4- Acetoxybutyl)malonic acid diethyl

ester (3) (5.0 g, 18.25 mmol) was taken in a 100 mL round-bottom flask containing methanol (50

mL) and stirred at room temperature for 2 min. To this solution, NaOH (2.1 g, 54.74 mmol) in

water (7 mL) was added and stirred at 90 ºC for 8 h. The reaction mixture was brought to room

temperature and acidified (pH 2-3) with the dropwise addition of dilute hydrochloric acid at room

temperature with constant stirring. The mixture was then concentrated using rotary evaporator

and applying vacuum. Chloroform (50 mL) was then added and Nitrogen gas was bubbled

through the solution at 60 ºC to remove excess HCl. The mixture was filtered and then

concentrated. This was then purified by column chromatography using 35% ethyl acetate in

petroleum ether as eluent.

Yield: 2.31 g (72%). ¹H NMR (300 MHz, CDCl₃, δ ppm, J Hz): 1.41 (m, 2H), 1.59 (m, 2H),

1.91 (q, 2H, J₁ = 7.3, J₂ = 7.8), 3.37 (t, 1H, J = 7.4), 3.64 (t, 2H, J = 6.5), 5.54 (bs, 1H). ¹³C NMR (75

MHz, CDCl₃, δ ppm): 23.53, 28.52, 31.75, 52.64, 62.11, 170.55. IR (CHCl₃): 3507, 2941, 1710,

1626, 1459, 1438, 1391, 1198, 1157, 1050, 947, 772, 741, 664 cm⁻¹.[1]

Synthesis of 2-(4-Hydroxybutyl)malonic Acid Diethylene Glycol PBPE Co-Polymer (7): 2-(4-

Hydroxybutyl)malonic acid (4) (0.63 g, 3.58 mmol) and diethylene glycol (5) (0.38 g, 3.58 mmol)

were added to a 5 mL round bottom flask (RBF) with a stir bar, then thoroughly mixed and

degassed to remove all dissolved oxygen and water, and put under an ultra-high purity (UHP)

nitrogen blanket. Freshly recrystallized catalyst ρ-tolulenesulfonic acid was then added in a

catalytic amount (100:1 molar ratio). After purging the RBF, a steady flow of UHP-N₂ gas was

flown over the reaction and lowered into an oil bath. Stirring commences and the reaction is

allowed to heat up to 140 ºC for 8 h. At this point a medium vacuum (1.5 mm/Hg) is introduced

to the reaction for 30 min. Next the vacuum is brought down to high vacuum (4 x 10^{-4} mm/Hg)

and polymerization continues for 12 h. The resulting digol co-polymer was purified by dissolving

in methanol and precipitating in DI water. This was then centrifuged, washed with DI water, and

dried in a vacuum oven at 40 ºC over high vacuum for 12 h to get pure polymer. The purified

digol co-polymer was highly viscous like molasses and was amber in color. The polymer was

soluble in methanol (MeOH), dimethyl sulfoxide (DMSO), dimethyl formamide (DMF),

tetrahydrofuran (THF), and chloroform (CHCl$_3$).

Yield: 56%. ^{1}H NMR (300 MHz, CDCl$_3$, δ ppm): 1.39 (m, 2H), 1.65 (m, 2H), 2.32 (m, 2H),

3.61 (m, 1H), 3.71 (m, 2H), 4.06 (m, 4H), 4.13 (m, 2H), 4.24 (m, 2H). ^{13}C NMR (75 MHz, CDCl$_3$, δ

ppm): 24.59, 28.39, 34.17, 51.85, 61.70, 62.56, 63.39, 64.21, 69.18, 72.49, 169.35, 173.62. IR:

3500, 2942, 2868, 1726, 1460, 1391, 1240, 1164, 1100, 1066, 905, 724, 649 cm^{-1}. TGA: 10%

weight loss at 265 ºC.

Synthesis of 2-(4-Hydroxybutyl)malonic Acid Triethylene Glycol PBPE Co-Polymer (8): 2-(4-

Hydroxybutyl)malonic acid (4) (0.54 g, 3.07 mmol) and triethylene glycol (6) (0.46 g, 3.07 mmol)

were added to a 5 mL round bottom flask (RBF) with a stir bar, then thoroughly mixed and

degassed to remove all dissolved oxygen and water, and put under an ultra-high purity (UHP)

nitrogen blanket. Freshly recrystallized catalyst ρ-tolulenesulfonic acid was then added in a

catalytic amount (100:1 molar ratio). After purging the RBF, a steady flow of UHP-N$_2$ gas was

flown over the reaction and lowered into an oil bath. Stirring commences and the reaction is

allowed to heat up to 140 ºC for 8 h. At this point a medium vacuum (1.5 mm/Hg) is introduced

to the reaction for 30 min. Next the RBF is evacuated to high vacuum (4 x 10^{-4} mm/Hg) and

polymerization continues for 12 h. The resulting digol co-polymer was purified by dissolving in methanol and precipitating in DI water. This was then centrifuged, washed with DI water, and dried in a vacuum oven at 40 ºC over high vacuum for 12 h to get pure polymer. The purified trigol co-polymer was highly viscous like molasses and was amber in color. The polymer was soluble in methanol (MeOH), dimethyl sulfoxide (DMSO), dimethyl formamide (DMF), tetrahydrofuran (THF), and chloroform (CHCl$_3$).

Yield: 52%. ^{1}H NMR (300 MHz, CDCl$_3$, δ ppm): 1.39 (m, 2H), 1.65 (m, 2H), 2.32 (m, 2H), 3.62 (m, 1H), 3.66 (m, 4H), 3.71 (m, 2H), 4.06 (m, 4H), 4.13 (m, 2H), 4.24 (m, 2H). ^{13}C NMR (75 MHz, CDCl$_3$, δ ppm): 24.62, 28.40, 34.19, 51.85, 61.78, 62.56, 63.40, 64.21, 69.25, 70.62, 72.61, 169.37, 173.60. IR: 3450, 2940, 2867, 1728, 1458, 1389, 1239, 1162, 1104, 1066, 904, 726, 649 cm^{-1}. TGA: 10% weight loss at 268 ºC.

Synthesis of Polymeric Nanoparticles: The polymer (30 mg) was placed in an Eppendorf tube and dissolved in DMSO (300 µL). Then doxorubicin (6 µL) was added to the polymer solution and vortexed for approximately 3 minutes at 1200 rpm. The resulting mixture was slowly added dropwise to a 15-mL Eppendorf tube containing DI water (4 mL) with continuous vortexing. Once the polymer-cargo mixture has been completely added to the water, the Eppendorf tube was capped, the vortex speed increased to 2500 rpm, and the solution was mixed for 1 h. The mixture was then transferred to a porous dialysis sleeve (MWCO= 3-6 kDa) for dialytic purification in DI water for 1 h. The drug-encapsulated nanoparticle was faintly pink in color (indicating doxorubicin was encapsulated), and was a stable solution free of precipitates.

To specifically target LNCaP prostate cancer cells, surface functional group modification so a targeting ligand can be attached is required. Surface modification can be achieved utilizing

carbodiimide chemistries to attach aminated folic acid (Fol-N_2). The folate ligand was chosen because of its specific binding and uptake by LNCaP cells (known to overexpress folate receptors on the surface of the cellular membrane. Synthesis and preparation of aminated folic acid is described and shown below in **Scheme 3**.
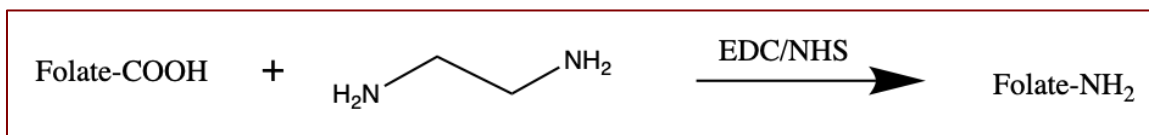
Scheme 3: *Synthesis of folate amine.*

Functionalizing the PBPE nanoparticles with folate starts with the synthesis of aminated folate. Folic acid (0.050 g, 22.1 mol) was added to a 5 mL Eppendorf tube with PBS buffer (2 mL). In a 1 mL Eppendorf tube, 1-Ethyl-3-(3-dimethylaminopropyl) carbodiimide (EDC) (0.02 g, 3.1 mol), N-Hydroxysuccinimide (NHS) (0.013 g, 1.5 mol), and 2-(N-morpholino) ethanesulfonic acid (MES) Buffer (0.5 mL, pH 5.0) were combined. The two solutions were combined and incubated at room temperature for 3 min. Then, 1,1-carbonyldiimidazole (CDI) (0.02 g, 3.2 mol) was dissolved in DMSO (0.1 mL), added dropwise to the PBPE-Doxo-COOH nanoparticle solution and incubated for 15 min. Finally, the folate/EDC/NHS solution (0.2 mL) was added dropwise to the PBPE-Doxo-COOH/CDI solution and incubated for 15 min. The mixture was then purified by dialysis in deionized water. The resulting folate-functionalized PBPE nanoparticles were now ready for incubation with the cancer cells.

FT-IR: Monomer or polymer samples (1- 5 mg) were placed in the PerkinElmer Spectrum 2 FT-IR spectrometer and scanned to gain their respective spectra. Monomer and polymer samples were vacuum-dried before analysis.

^{1}H NMR: Samples of each monomer (5-10 mg) or polymer (50 mg) were dissolved in DMSO-d_6 or CDCl$_3$ (750 μL) and processed in the Bruker DPX-300 MHz spectrometer using the TOPSPIN 1.3 program for 24 scans with a T_2 delay of 10 s. Monomer and polymer samples were vacuum-dried before dissolving in the deuterated solvent.

^{13}C NMR: Samples of each monomer and polymer (40-50 mg) were dissolved in DMSO-d_6 or CDCl$_3$ (750 μL) and processed in the Bruker DPX-300 MHz spectrometer using the TOPSPIN 1.3 program for 10000 scans. Monomer and polymer samples were vacuum-dried before dissolving in the deuterated solvent.

Gel Permeation Chromatography (GPC): Gel permeation chromatography (GPC) was performed with a Waters 2410 DRI gel permeation chromatograph, consisting of four phenogel 5 μL columns filled with cross-linked polystyrene-divinylbenzene (PSDVB) beads. The polymer samples (20 mg) were vacuum-dried, dissolved in butylated hydroxytoluene (BHT)-stabilized THF (1 mL), filtered through a 0.2 μm filter and then transferred to a GPC vial. The eluent flow rate of tetrahydrofuran (THF) was set to 1 mL/min at 30 ºC for 50 minutes.

Matrix-Assisted Laser Desorption/Ionization-Time of Flight (MALDI-TOF): MALDI-TOF was performed on the Bruker microflex™ LRF MALDI-TOF. The matrix for the samples was prepared

per the protocol provided in the Bruker user manual. First, TA30 solvent (30:70 volume ratio of acetonitrile in DI water to 0.1% trifluoroacetic acid) was prepared in 100 μL quantity. Then 2,5-dihydroxybenzoic acid (2 mg) was dissolved and mixed in the TA30 to complete the matrix solution. Next, the polymer sample (5 mg) was vacuum dried, then dissolved in methanol (100 mL). 100 μL of each solution (the polymer solution and the TA30 matrix solution) were combined in a 1 mL Eppendorf tube and vortexed (1000 rpm) for 2 min to ensure complete mixing. The resulting solution was then spotted (1 μL drop size) in the wells of a ground steel MALDI target plate. The spots were left to dry completely (approximately 6 h) and placed in the mass spectrometer for analysis.

Thermogravimetric Analysis (TGA): Thermal stability of the polymers were tested on a TA Instruments Q50 thermogravimetric analyzer. Polymer samples of about 10 mg were weighed and then heated under a nitrogen atmosphere using a ramp rate of 10 ºC/min for 60 minutes, ranging from 25 – 600 ºC.

Differential Scanning Calorimetry (DSC): The calorimetric parameters of the polymer were analyzed on a TA Instruments Q100 differential scanning calorimeter. Polymer samples of about 10 mg were used for the test. The device was set to one cycle ranging from -80 – 120 ºC with a ramp rate of 10 ºC/min.

Dynamic Light Scattering and Zeta Potential: The polymeric nanoparticle (10 μL) solution was added to deionized water (1 mL). This solution was then placed in a standard cuvette for DLS reading, or a specialized electrode-containing cuvette for zeta potential determination. The appropriate cuvette was placed in the Malvern ZS90 zetasizer and the program set up (approximately 50 readings in 3 cycles) for the appropriate data acquisition.

UV/Vis and Fluorescence Analysis: UV/Vis spectra were documented using a Tecan infinite M200 Pro microplate reader. Samples of polymeric nanoparticle suspension (50 μL) were placed in a 96-well plate and inserted in the spectrophotometer. Absorbance scans were set to a range of 300-800 nm and fluorescence emission scans were set to wavelengths of 600-900 nm. Readings were taken at intervals of 5 nm, with 10 flashes for each reading. The resulting data points were transferred to Microsoft Excel and plotted using a smooth line scatter plot to visualize and compare the samples.

Cell Studies

Cell Culturing: LNCaP and PC3 prostate cancer cells were grown in a specially formulated media containing, by volume, 85% RPMI-1640 media, 10% fetal bovine serum, and 5% Penicillin/Streptomycin antibiotic. These components were mixed, vacuum-filtered, and stored at 4°C until needed. The cells taken from cryo were re-suspended in this media (5 mL), transferred to a 7-mL culture flask, and incubated at 37°C. Cells were split to new flasks with fresh media as needed to prevent overcrowding and to increase the longevity of the cells. Cell samples used for assays were taken from flasks with the most recently changed media and at least 24 hours old, or roughly 80% confluent.

MTT Assay: Fresh cells were cultured in a 96-well plate and incubated with 50 μL dosages of the polymeric nanoparticle formulations (both with and without folic acid and doxorubicin) for 24 hours. After incubation the media was removed and 50 μL of 1X PBS was added to the cells for washing. The PBS was removed, then 25 μL of the MTT solution (50 mg MTT in 10 mL 1X PBS) was added to the wells and further incubated for 4-6 hours. Following MTT incubation, the excess

MTT solution was drained from the wells and 30 μL of isopropanol was added. The cells were

then ready to be read in the TECAN Infinite M200 PRO multi-detection microplate reader (at 560

nm absorbance) to determine the cytotoxicity of the nanoparticle treatment.

References

(1)   Santra, S.; Kaittanis, C.; Perez, J. M. *Langmuir* **2010**, *26* (8), 5364–5373.

(2)   Britannica, E. O. E. *Monomer*; Encyclopedia Britannica, Inc., 2015.

(3)   Britannica, E. O. E. *Polymer*; Encyclopedia Britannica, Inc., 2019.

(4)   Staudinger, H. *Berichte der deutschen chemischen Gesellschaft (A and B Series)* **1920**, *53* (6), 1073–1085.

(5)   Staudinger, H. *Trans. Faraday Soc.* **1933**, *29* (140), 18–32.

(6)   Mülhaupt, R. *Angewandte Chemie International Edition* **2004**, *43* (9), 1054–1063.

(7)   Young, R. J.; Lovell, P. A. *Introduction to polymers*; CRC Press: Boca Ratón, 2011.

(8)   Ghosh, P. *Polymer Science and Technology*; McGraw-Hill Education LLC, 1990.

(9)   Zhao, W.; Jin, X.; Cong, Y.; Liu, Y.; Fu, J. *Journal of Chemical Technology & Biotechnology* **2013**, *88* (3), 327–339.

(10)   Dang, J.; Leong, K. *Advanced Drug Delivery Reviews* **2006**, *58* (4), 487–499.

(11)   Cascone, M. G.; Sim, B.; Sandra, D. *Biomaterials* **1995**, *16* (7), 569–574.

(12)   Ouellette, R. J.; Rawn, J. D. In *Organic Chemistry Study Guide*; Elsevier, 2015; pp 587–601.

(13)   Malikmammadov, E.; Hasirci, N. In *Smart Polymers and their Applications*; Elsevier, 2019; pp 255–278.

(14)   Abbasi, E.; Aval, S.; Akbarzadeh, A.; Milani, M.; Nasrabadi, H.; Joo, S.; Hanifehpour, Y.; Nejati-Koshki, K.; Pashaei-Asl, R. *Nanoscale Res Lett* **2014**, *9* (1), 247.

(15)   Zheng, Y.; Li, S.; Weng, Z.; Gao, C. *Chem. Soc. Rev.* **2015**, *44* (12), 4091–4130.

(16)   Hoare, T. R.; Kohane, D. S. *Polymer* **2008**, *49* (8), 1993–2007.

(17)   *Dendrimers and Other Dendritic Polymers*; Fréchet, J. M. J., Tomalia, D. A., Eds.; John Wiley & Sons, Ltd: Chichester, UK, 2002; pp 1–44.

(18)   Acharya, G.; Mitra, A. K.; Cholkar, K. In *Emerging Nanotechnologies for Diagnostics, Drug Delivery and Medical Devices*; Elsevier, 2017; pp 217–248.

(19)   Caballero-George, C.; Marin; Briceño. *IJN* **2013**, *8* (1), 3071–3091.

(20)   La Du, B. N.; Snady, H. *Concepts in Biochemical Pharmacology*; Brodie, B. B., Gillette, J. R., Ackerman, H. S., Eds.; Springer Berlin Heidelberg: Berlin, Heidelberg, 1971; Vol. 28, pp 477–499.

(21)   Li, S.; Vert, M. In *Degradable Polymers*; Springer Netherlands: Dordrecht, 2002; pp 71–131.

(22)   Heckert, B.; Banerjee, T.; Sulthana, S.; Naz, S.; Alnasser, R.; Thompson, D.; Normand, G.; Grimm, J.; Perez, J. M.; Santra, S. *ACS Macro Lett.* **2017**, *6* (3), 235–240.

(23)   Children's Hospital of Philadelphia. *Phys.org*. Philadelphia April 2, 2015.

(24)   Steichen, S. D.; Caldorera-Moore, M.; Peppas, N. A. *European Journal of Pharmaceutical Sciences* **2013**, *48* (3), 416–427.

(25)   Feng, L.; Dong, Z.; Tao, D.; Zhang, Y.; Liu, Z. *Natl Sci Rev* **2018**, *5* (2), 269–286.

(26)   Cook, J. A.; Gius, D.; Wink, D. A.; Krishna, M. C.; Russo, A.; Mitchell, J. B. *Seminars in Radiation Oncology* **2004**, *14* (3), 259–266.

(27)   Santra, S.; Kaittanis, C.; Santiesteban, O. J.; Perez, J. M. *J. Am. Chem. Soc.* **2011**, *133* (41), 16680–16688.

(28)   Boohaker, R. J.; Zhang, G.; Lee, M. W.; Nemec, K. N.; Santra, S.; Perez, J. M.; Khaled, A. R. *Mol. Pharmaceutics* **2012**, *9* (7), 2080–2093.

(29)   Sulthana, S.; Banerjee, T.; Kallu, J.; Vuppala, S. R.; Heckert, B.; Naz, S.; Shelby, T.; Yambem, O.; Santra, S. *Mol. Pharmaceutics* **2017**, *14* (3), 875–884.

(30)   van Meerloo, J.; Kaspers, G. J. L.; Cloos, J. In *Cancer Cell Culture*; Methods in Molecular Biology; Humana Press: Totowa, NJ, 2011; Vol. 731, pp 237–245.

(31)   Santra, S.; Kaittanis, C.; Perez, J. M. *Mol. Pharmaceutics* **2010**, *7* (4), 1209–1222.